Epigenomic landscape of the human dorsal root ganglion: sex differences and transcriptional regulation of nociceptive genes

Running title: epigenome of the human DRG

Úrzula Franco-Enzástiga[1], Nikhil N. Inturi[1], Keerthana Natarajan[1], Juliet M. Mwirigi[1], Khadija Mazhar[1], Johannes C.M. Schlachetzki[2], Mark Schumacher[3], Theodore J. Price[1,*]

[1] Center for Advanced Pain Studies, School of Behavioral and Brain Sciences, University of Texas at Dallas, Richardson, Texas 75080.

[2] Department of Cellular and Molecular Medicine, University of California, San Diego, 9500 Gilman Drive, La Jolla, CA 92093-0651, USA.

[3] Department of Anesthesia and Perioperative Care and the UCSF Pain and Addiction Research Center, University of California, San Francisco, California, 94143 USA.

[*]Correspondence to:

Theodore J Price PhD
800 W Campbell Rd
BSB14.102
Richardson TX 75080
USA
theodore.price@utdallas.edu
+1 972-883-4311

Word count: 12,376
Abstract: 210
Number of Text Pages: 40
Number of Figures: 8 (Supplementary figures: 4)
Number of Tables: 0 (Supplementary tables: 7)
Number of Datasets: 5

Key words - epigenetics, dorsal root ganglion, ATAC-seq, sex differences, XIST, EGR1

Author Contributions – UFE and TJP designed research project; UFE conducted ATAC-seq and RNA-seq experiments; UFE, NNI, and JCMS performed computational analysis; UFE and KN performed *in situ* hybridization experiments; JM and KM supplied computational feedback; JCMS and MS provided insight to the paper; UFE and TJP wrote the paper.

Abstract:

Gene expression is influenced by chromatin architecture via controlled access of regulatory factors to DNA. To better understand gene regulation in the human dorsal root ganglion (hDRG) we used bulk and spatial transposase-accessible chromatin technology followed by sequencing (ATAC-seq). Using bulk ATAC-seq, we detected that in females diverse differentially accessible chromatin regions (DARs) mapped to the X chromosome and in males to autosomal genes. EGR1/3 and SP1/4 transcription factor binding motifs were abundant within DARs in females, and JUN, FOS and other AP-1 factors in males. To dissect the open chromatin profile in hDRG neurons, we used spatial ATAC-seq. The neuron cluster showed higher chromatin accessibility in GABAergic, glutamatergic, and interferon-related genes in females, and in Ca^{2+}-signaling-related genes in males. Sex differences in transcription factor binding sites in neuron-proximal barcodes were consistent with the trends observed in bulk ATAC-seq data. We validated that *EGR1* expression is biased to female hDRG compared to male. Strikingly, *XIST*, the long-noncoding RNA responsible for X inactivation, hybridization signal was found to be highly dispersed in the female neuronal but not non-neuronal nuclei suggesting weak X inactivation in female hDRG neurons. Our findings point to baseline epigenomic sex differences in the hDRG that likely underlie divergent transcriptional responses that determine mechanistic sex differences in pain.

Introduction

Women exhibit a higher prevalence of chronic pain [53], a greater number of clinical pain conditions [5], and a heightened sensitivity to experimental pain compared to men [24]. The strongest evidence is epidemiological and mechanistic sex differences in chronic pain conditions [45-47; 62]. Neuropathic, inflammatory and idiopathic chronic pain have higher prevalence rates, symptom severity and duration in women compared to men [16; 47; 78]. Although hormonal, immunological, anatomical and psychosocial factors contribute to sex differences in pain [55], at least some of these differences are likely driven by sex-specific gene expression in sensory neurons, glia or immune cells of the human dorsal root ganglion (hDRG). Support for this idea comes from animal model work demonstrating distinct mechanisms that promote and resolve chronic pain in rodents [20; 25]. Mechanistic studies in humans demonstrate sex differences in gene expression for transcription factors and epigenetic remodelers in hDRG from thoracic vertebrectomy patients suffering from chronic pain [50; 59]. Moreover, in both the human tibial nerve and in the human DRG, as well as in the mouse DRG, there are sex differences in gene expression in individuals without any pain history suggesting underlying epigenetic differences at baseline that cause these divergent patterns of gene expression [36; 42; 50; 58; 59; 75; 76].

Chromatin is a macromolecular complex composed of DNA, RNAs, and proteins found within the nuclear space. Epigenetic marks, such as specific histone or DNA modifications, can affect the degree of DNA compaction resulting either in open or accessible regions termed euchromatin or closed compact regions known as heterochromatin [3]. Chromatin accessibility is defined as the extent to which nuclear macromolecules can physically interact with chromatinized DNA [31]. Although chromatin serves a structural role by compacting DNA, it is also a dynamic entity that responds to cellular needs such as transcription, DNA repair, and differentiation [39; 44]. These dynamic changes in chromatin have been shown in the DRG in animal models in response to nerve injury and to inflammation, demonstrating a functional link between epigenomic regulation of gene expression and development and maintenance of chronic pain [9; 21; 34; 37; 41; 72; 80; 81]. To date very little is known about

chromatin accessibility in hDRG although one previous study using microarray-based genomic and mRNA expression profiling found that expression quantitative trait loci were associated with open chromatin regions based on encyclopedia of DNA elements datasets [52]. A study of the human trigeminal ganglion (TG) found association between single nucleus ATAC-seq (snATAC-seq) open chromatin regions and single nucleotide polymorphisms (SNPs) associated with migraine [88]. However, the degree to which SNPs linked to migraine could be correlated to open chromatin in human TG cells was limited because snATAC-seq failed to cover all TG cell types detected with snRNA-seq.

We hypothesized that epigenomic differences in the hDRG may underlie mechanistic differences in molecular events that promote pain in females versus males and contribute to the higher propensity for women to develop chronic pain disorders. As a first test of this idea, we used both bulk and spatial ATAC-seq coupled with bulk nuclear RNA-seq to map the open chromatin accessibility landscape of DRG in female and male organ donor-recovered tissues. We found pervasive differences in transcriptional regulatory programs between females and males that likely have important implications for understanding epidemiological and mechanism-based differences in chronic pain in humans.

Materials and methods

DRG tissue preparation

All human tissue procurement procedures were approved by the Institutional Review Board at the University of Texas at Dallas. Lumbar DRGs from human organ donors were obtained via a collaborative effort with the Southwest Transplant Alliance. Right after dissection, human L4 or L5 DRGs from male and female organ donors were either transported in aCSF to be further processed within our facilities or frozen in dry ice right after dissection and stored in a −80 °C freezer. DRG donor demographic information is provided in **Table S1**. The inclusion criteria for this study took into account adult donors aged 18 to 65 years who exhibited no signs of pain or neuropathy. The cutoff age of 65 years old was determined based on prior epigenomic studies, which indicated

significant alterations in both males and females occurring notably after the age of 65 [40].

Bulk ATAC-seq on fresh hDRG

Immediately after dissection, human L4 or L5 DRGs from male and female organ donors were transported in cold bubbled NMDG-aCSF pH 7.4 (93 mM NMDG, 2.5 mM KCl, 1.25 mM NaH_2PO_4, 30 mM $NaHCO_3$, 20 mM HEPES, 25 mM glucose, 5 mM ascorbic acid, 2 mM thiourea, 3 mM sodium pyruvate, 10 mM Mg_2SO_4, 0.5 mM $CaCl_2$, 12 mM N-acetylcysteine; osmolarity 310 mOsm [82] in ice to our facilities. Using scissors, tissue was chopped in 2 mL of ice-cold nuclei isolation buffer [43]. This buffer contained: 250 mM sucrose, 25 mM KCl, 5 mM $MgCl_2$, 10 mM Tris-HCl pH 8.0 and 0.1% triton X-100. The total volume was transferred to a Dounce homogenizer. 5 strokes of the loose pestle and 15 strokes of the tight pestle were applied. The homogenate was transferred to a conical tube and centrifuged at 100 x g for 8 min at 4 °C. The supernatant was carefully removed without disrupting the soft pellet. Next, the pellet was resuspended in 2 mL of nuclei isolation buffer free of triton. The supernatant was removed without disrupting the pellet after centrifugation at 100 x g for 8 min at 4 °C. Subsequently, the nuclei were resuspended in 2 mL of nuclei isolation buffer without triton and filtered through a 40-um cell strainer. The number of isolated nuclei was counted using a hematocytometer. A total of 100,000 nuclei were aliquoted and centrifuged at 500 x g for 10 min at 4 °C. The supernatant was then removed, and the pellet was utilized for the tagmentation reaction and DNA purification using the Active Motif kit (Cat. No. 53150). In brief, 50 uL of Tagmentation Master Mix (consisting of 2X Tagmentation buffer, 10X PBS, 0.5% digitonin, 10% tween 20, and assembled transposomes) was added to each sample. The tagmentation reaction was incubated at 37 °C for 30 min in a thermomixer at 800 rpm. Subsequently, 250 uL of purification binding buffer and 5 uL of 3 M sodium acetate were added. DNA purification columns were employed to isolate the DNA, and the tagmented DNA was eluted in 35 uL of DNA elution buffer. The amplification of tagmented DNA through PCR was carried out using i7- and i5-Illumina's Nextera-based adapters as per the provider's instructions. Pair-end

75 cycle sequencing reads were acquired on the Nextera500 sequencer or Nextera2000 sequencer. A total of 100 million reads were obtained from each sample.

RNA-seq on fresh hDRG

After isolating 100,000 nuclei from hDRG for bulk ATAC-seq, the remaining extracted nuclei were used to perform RNA extraction with the aim of sequencing and pairing bulk nucRNA-seq with ATAC-seq from the same sample. Four male and 3 female hDRG samples were utilized to extract RNA, thus the pairing with ATAC-seq samples was performed in 6 out of 10 ATAC-seq samples.

Total RNA from hDRG nuclei was purified using TRIzol™. RNA peak profiles were analyzed using 5200 Fragment Analyzer and quantified with Qubit. RNA quality number was used to assess RNA Integrity (**Table S2**). Illumina Tru-seq stranded RNA library prep was used to generate cDNA libraries according to the manufacturer's instructions. Next Generation Sequencing (RNA-seq) was performed in a NextSeq 2000 sequencer. Single-end sequencing was performed in a multiplexed fashion by loading the samples on a P2 flow cell, averaging ~50 million reads per sample.

Spatial ATAC-seq on frozen hDRG

The frozen hDRGs were gradually embedded in OCT in a cryomold by adding small volumes of OCT over dry ice to avoid thawing. A total of 8 hDRGs were used for these experiments (N=3 female, N=5 male) and demographic information of the organ donors is provided in **Table S3**. All tissues were cryostat sectioned at 10 µm onto SuperFrost Plus charged slides (Fisher Scientific; Cat 12–550-15). Sections were only briefly thawed in order to adhere to the slide but were immediately returned to the −20 °C cryostat chamber until completion of sectioning. The slides were removed from the cryostat and sent to AtlasXomics for further processing [13]. Spatial ATAC-seq (AXO-0303) consisted of the next steps: the tissue was fixed for 5 min with 0.2% paraformaldehyde. Afterwards, the tissue was treated with glycine and left to dry. Then, a tissue permeabilization step was performed using 0.1% NP40 for 15 minutes. Tn5 transposition on the fixed hDRG sections was carried out for 30 min. Adapters

containing a ligation linker were added to the preparation to be inserted in accessible genomic loci. Barcodes with linkers were introduced using microchannels and were ligated to the 5′ end of the Tn5 oligo through successive rounds of ligation. hDRG sections were imaged to correlate spatially barcoded accessible chromatin with tissue morphology. A barcoded-tissue mosaic was created, reverse cross-linking was performed to release DNA-fragment, which were then amplified through PCR for subsequent library preparation. 150X150 paired-end sequencing was performed using NextSeq 2000 with 15% PhiX. Sequencing depth was up to 300 million reads per sample.

Processing of bulk ATAC-seq data

First, we verified the quality of raw sequencing fastq files using FastQC v0.11.7. We removed adapters using TrimGalore-0.6.6 and verified the quality of trimming using FastQC v0.11.7. Paired-end reads were mapped to the reference genome GRCh38/hg38 using Bowtie2. To remove unmapped reads, low quality reads or reads that mapped to mitochondrial DNA and PCR duplicates we used Bamtools. Areas of open chromatin were identified by peak calling for each sample using Macs2 v.2.2.7.1 in keeping with Galaxy ATAC-seq data analysis. Differential accessibility between male and female donors was analyzed using DiffBind, a package within the Bioconductor framework. During differential analysis, normalization was performed in a default mode. Next, we used HOMER annotatePeaks which uses the program assignGenomeAnnotation to efficiently assign ATAC-seq peaks to genomic annotations. The definitions of annotations were acquired in a default mode. Processing of transcription factor binding sites was performed using Transcription factor Occupancy prediction By Investigation of ATAC-seq Signal (TOBIAS, [4]) in conjunction with human consensus transcription factor motifs from JASPAR. In brief, ATACorrect parameter was used to assess and correct the Tn5 transposase sequence preference of cutting sites. Putative transcription factor binding sites or transcription factor occupancy within peak regions were estimated using FootprintScore. Differential transcription factor binding sites in ATAC-seq reads between male and female hDRG were detected with

BINDetect. Differentially Accessible Regions (DARs) were identified using DESeq2 v1.42.0.

Processing of RNA-seq data

We confirmed the quality of raw sequencing fastq files using FastQC v0.11.7. The STAR alignment tool (v2.7.10b) was employed for aligning sequenced reads to the human GENCODE reference genome (v38). Sequenced reads underwent trimming to reduce sequencing quality issues at both ends. Relative abundance quantified as TPM was generated using the Stringtie tool and HTseq for counts generation.

Processing of spatial ATAC-seq data

Processing of spatial ATAC-seq was performed by AtlasXomics, as previously reported [13]. Chromap was used to perform the alignment of sequenced reads to the human GENCODE reference genome (v38) and remove duplicates from fastq files [91]. Fragments files containing coordinates of sequenced DNA molecules mapping to barcodes were generated for downstream analysis. For data visualization, pixels on tissue samples were designated using AtlasXbrowser based on microscopy images to create Seurat-compatible metadata files. ArchR was used to process fragments files and the remotion of pixels not on tissue were removed. Data normalization and dimensionality reduction was applied to the data using ArchR's iterative latent semantic indexing and subsequent graph clustering and Uniform Manifold Approximation and Projection (UMAP) embedding were performed. ArchR functions were used to acquire gene accessibility scores and matrices (gene score model), marker genes for clustering, and genome browser tracks. ShinyGO-080 was used to plot chromosomal location of DARs-associated genes to the human genome.

***In situ* hybridization**

hDRGs from non-pain donors were embedded in OCT using a cryomold over dry ice and sectioned. 10 µm sections for *XIST* and 20 µm sections for *EGR1* detection were placed onto SuperFrost® Plus charged slides (Thermo Fisher Scientific, cat. No. 1255015). Two sections per hDRG separated by at least 100 µm from each other were obtained to capture two sets of neurons allowing for a diverse population to be

analyzed. Sections were fixed in cold 10% formalin pH 7.4 for 15 min and then dehydrated sequentially in 50% ethanol for 5 min, 70% ethanol for 5 min, and 100% ethanol for 10 min at RT. The slides were allowed to dry briefly and hydrophobic boundaries around the tissue sections were drawn with ImmEdge® PAP pen (Vector Laboratories cat. no. H-4000). RNAScope® Fluorescent Multiplex Reagent Kit (Advanced Cell Diagnostics (ACD), cat. no. 323100) was used to detect target *EGR1* (ACD, cat. no. 457671), *XIST* (ACD, cat. no. 311231) and *SCN10A* (ACD, cat. no. 406291-C2) mRNAs in hDRGs. The sections were treated with hydrogen peroxide (ACD, cat. no. 322335) for 10 min at RT followed by a rinse with ddH_2O. Sections then underwent 5 s of protease III (ACD, cat. no. 322337) digestion followed by a quick wash in 1X PBS at RT. *EGR1* or *XIST* (Channel 1) and *SCN10A* (Channel 2) probes were mixed in 50:1 ratio. The probe solution was added to the sections placed onto the HybEZ™ Slide Rack (ACD, cat. no. 310017) which was then placed inside the HybEZ™ tray (ACD, cat. no. 310012). Probes were hybridized at 40°C for 2 h in HybEZ™ II Oven (ACD, cat. no. 321721). Sections were rinsed twice in 1X RNAScope® Wash Buffer (ACD, cat. no. 310091) at RT for a couple of minutes each. The sections were stored in 5X SSC buffer (Sigma-Aldrich, cat. no. S6636) overnight at RT. The slides were rinsed twice with 1X wash buffer followed by amplification with Amp 1 for 30 min, Amp 2 for 30 min, and Amp 3 for 15 min at 40°C. Channel 1 probe was coupled with Cy3 for *EGR1* or *XIST* detection and channel 2 with Cy5 for *SCN10A* detection. After rinsing two times with 1X wash buffer, sections were incubated with 1:5000 DAPI in 1X PBS for 1 min. Tissue sections underwent a rinse with 1X PBS before being air-dried completely and cover-slipped with ProLong™ Gold Antifade Mountant (Fisher Scientific cat. no. P36930). Slides were imaged at 20X, 60X and 100X magnification using the Olympus FV3000 RS confocal laser scanning microscope. In situ hybridization analysis was performed using ImageJ Fiji version 2.14.0 by Difference of Gaussians (DoG) edge detection method. For EGR1 analysis, ROIs were hand-drawn around each neuron avoiding lipofuscin on the image hyper stack. Channels with target probe were separated from the hyper stack and duplicated. The two images underwent the application of Gaussian Blur with sigma values 1 and 2 respectively. The two resulting images with blurs were subtracted using the built-in Image Calculator feature in ImageJ

Fiji which allowed for detection of in situ hybridization puncta using the default threshold function. Thresholding values that allowed for as little noise as possible without compromising the signal were chosen for each channel. Analyze Particles feature was used to analyze the number of puncta. The count readout was extracted from the images across the 10 donors which were then used to plot *EGR1* puncta count in *SCN10A* positive or negative neurons for each sex. *EGR1* puncta count data are presented as violin plots with thick line indicating the median and the dotted lines indicating the quartiles. Data were analyzed with Graphpad Prism V9 (Graphpad, San Diego, CA). Student's t test was used to assess differences in puncta count between sexes. A $p<0.05$ was considered statistically significant. Donor information for these experiments is provided in **Table S4**. For *XIST* analysis, ROIs were hand-drawn around analyzed nuclei using DAPI as a guide. Dispersal of *XIST* was measured based on dispersion of hybridization signal puncta in hand-draw ROIs that traced the analyzed nuclei. This area was divided by the total nuclear area stained with DAPI. Donor information for these experiments is provided in **Table S5**.

Results

Global chromatin landscape in female and male hDRG

To characterize the epigenetic landscape of the hDRG we performed ATAC-seq [8], an unbiased approach to assess chromatin accessibility regions within the genome [65] on lumbar hDRG from 9 donors (N=5 females, N=4 males, **Fig. 1A**). Donor information for all the samples that were used for bulk-ATAC in hDRG is shown in **Table S1**. After peak calling, we obtained a total of 669,749 peaks in female and 506,435 in male hDRG samples. At the global level, the distribution of called peaks in both female and male hDRG samples is concentrated in close proximity to the Transcription Start Site (TSS), with a notable accumulation of ATAC-seq signal directly at the TSS rather than in the immediate vicinity (**Fig. 1B**). The ratio between aggregate distribution of reads centered around the TSS (± 1 kb) and the signal flanking it is referred to as TSS enrichment (TSSe) score. TSSe is an important quality control parameter in ATAC-seq. We obtained a mean TSSe of 3.17 (**Fig. 1C**) similar to other reports using postmortem human tissue [10; 26]. Fragments of peaks in peaks (FRiP) defined as the measure of

how many of the total reads are located within the peaks was greater than 0.13 in average. By mapping ATAC-seq peaks to genomic regions, we found that ~15% of peaks mapped within the putative promoter, ~40% were in distal intergenic regions, and ~35% were found in introns (**Fig. 1D**). The enrichment of accessible chromatin in intergenic regions suggests that distal regulatory sequences, such as enhancers, non-coding regulatory elements in *cis*, can be accessed to regulate gene expression. In many cases, peaks located mainly in promoters [70], but also those harbored in the gene body (introns and exons) have been found to be good predictors of gene expression [23]. However, the proof of concept for the functionality of enhancers is tissue specific and requires further experimentation [77]. Since our results show that, at the global level, chromatin accessibility in hDRG showed similar annotation to called peaks between sexes, and the proportion was typical to other ATAC-seq reports [87], we aimed to conduct a sex-specific analysis identifying specific genes to investigate whether sex differences in pain could be associated with chromatin structure.

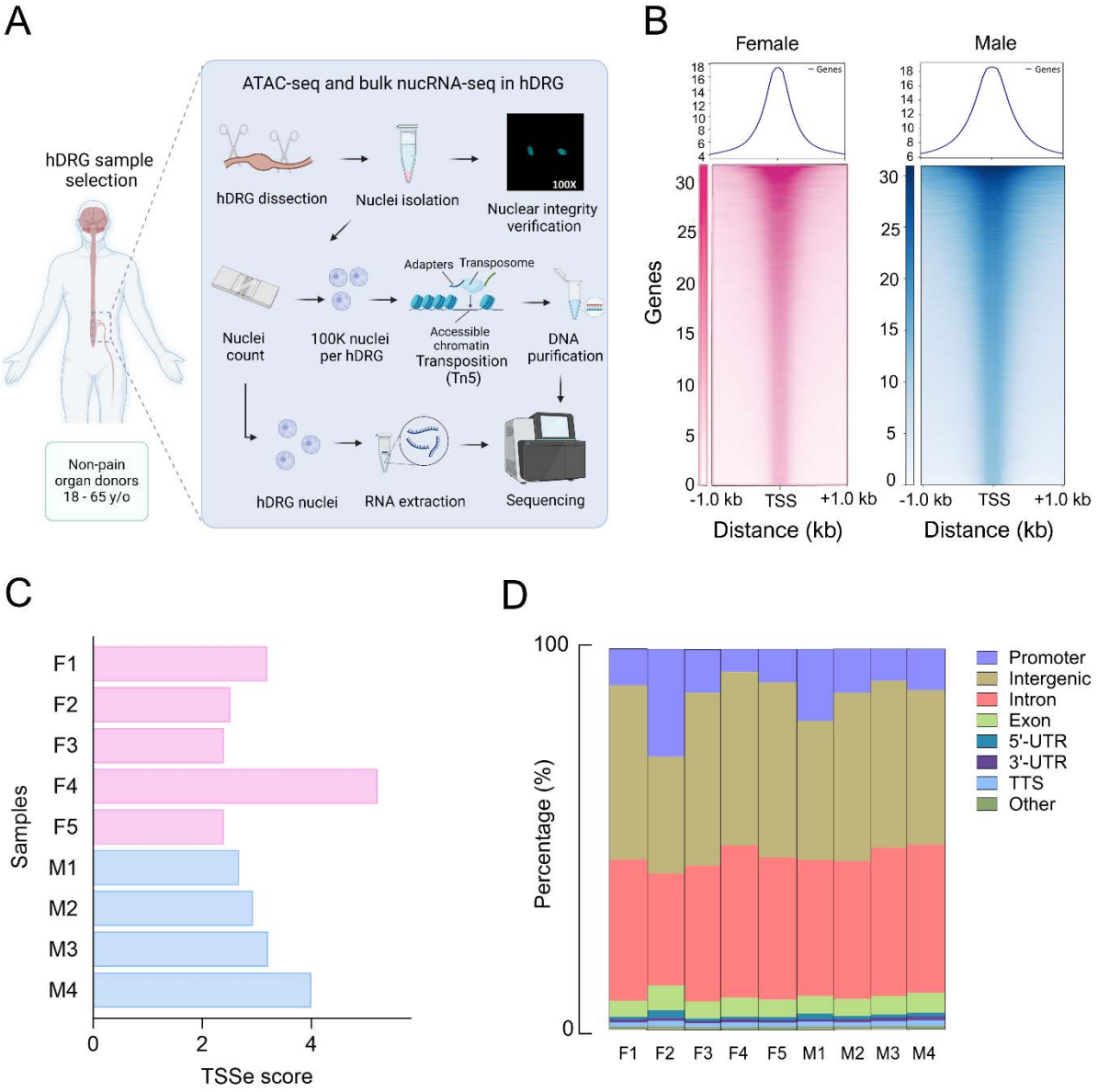

Figure 1. *Uncovering the open chromatin landscape in hDRG*. **A)** Schematic of the study design for bulk ATAC-seq. **B)** Heatmap shows chromatin accessibility around TSS ± 1 kb using aggregated peak enrichment scores from different female or male hDRG samples. Each row represents one consensus peak per gene spanning the TSS ordered by ATAC-seq signal intensity. Color represents the intensity of normalized chromatin accessibility. The metaplot on the top shows the mean ATAC-seq signal at the TSS. **C)** TSSe score obtained for each sample as a QC metric. **D)** Proportion of

ATAC-seq peaks associated with different genomic annotations in each hDRG sample (UTR = untranslated region; TTS = Transcription Termination Site).

Sex differences in chromatin accessibility in hDRG

By comparing ATAC-seq peaks in female and male samples, we found 3005 differentially accessible chromatin regions (DARs, FDR < 0.01, **Fig 2A**; complete DAR list is supplied in **Dataset S1**). Among these, 41 were identified in gene promoters in the female hDRG. Notably, the majority of DARs were located on the X chromosome in genes such as *MAPD72*, *FRMPD4, PORCN, PNMA3* and *TKTL1* (**Fig. 2A**). In males, 234 DARs were associated with gene promoters (±1kb from TSS) on autosomal chromosomes and included genes such as *NR1D1*, *IRF2*, *CCNB1*, *DAPK3* and *FOXO1* (**Fig. 2A,** promoter DAR list is supplied in **Dataset S2**). The ATAC-seq principal component analysis (**Fig. 2B**) demonstrated that female and male samples clustered separately, consistent with the DAR analysis results. Representative sex biased DARs around the TSS in female and male hDRG are shown in **Fig. 2C** and **D**, respectively. X inactivation is known to balance X chromosome gene expression between sexes, although it is incomplete in some tissues and new regulatory functions associated with escape from X inactivation are still being discovered [64]. We observed a striking number of DARs in this chromosome in the female DRG likely consistent with a lack of X silencing in the hDRG in females or the presence of poised genes ready to be activated. X inactivate-specific transcript (*XIST*), the long non-coding RNA (lncRNA) that primarily functions to silence one of the X chromosomes in each female cell, has been found to be dysregulated and participate in inflammatory and chronic pain in animal models [35; 68; 73; 83], suggesting a possible X inactivation dysregulation which could become more relevant in pathological conditions.

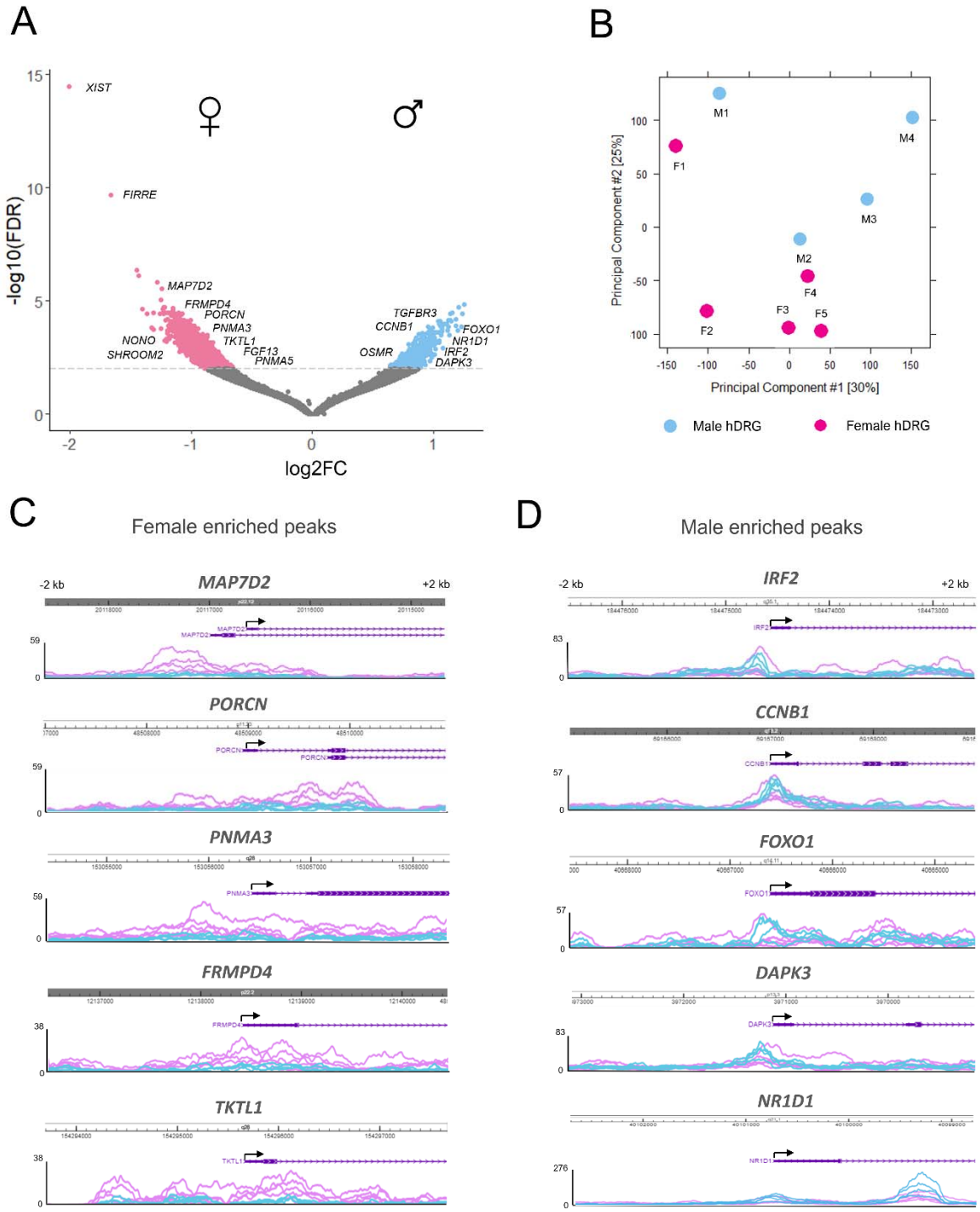

Figure 2. *Analysis of sex differences in open chromatin regions in hDRG*. **A)** Volcano plot showing DARs in hDRG between sexes (N = 9, 5 female (pink), and 4 male (blue) postmortem hDRGs, FDR < 0.01) identified with Diffbind. **B)** Principal component plot for ATAC-seq samples based on their similarity. **C)** Genome browser views of ATAC-

seq signal of DARs surrounding the transcription start site from female hDRG. **D)** Representative genome browser tracks of DARs surrounding the transcription start site in male hDRG.

Enriched transcription factor binding sites in sex-biased DARs in hDRG

In addition to chromatin accessibility, ATAC-seq data enables the prediction of transcription factor binding to open chromatin regions. With the aim of dissecting sex-specific transcriptional activity programs in hDRG, we analyzed the differential transcription factor binding motifs within accessible chromatin between sexes in hDRG using Transcription factor Occupancy prediction By Investigation of ATAC-seq Signal (TOBIAS). For this analysis, differential binding scores with - log10 (p-value) larger than the 95th percentiles (top 5% in each direction) were considered as significant [4]. In females, transcription factors of the EGR family such as EGR1 and EGR3, and members of the SP family such as SP1, SP2, SP4 and SP9 footprints were more abundant compared to male. In males, we found a higher level of footprints for transcription factors that are part of the activating protein 1 (AP-1) family such as JUN, FOS, FOSL2 and ATF4. (**Fig. 3A-B**). Binding of transcription factors to the promoter of specific accessible genes was also an output of TOBIAS analysis. We found that the EGR1 transcription factor has binding sites in *ADORA2B*, a synaptic-localized GPCR gene; *CX3CL1*, a chemokine known to participate in paclitaxel-induced macrophage recruitment in the DRG [27]; and *JAK1*, a kinase essential for cytokine and growth factors signal transduction. EGR3 showed open chromatin binding sites in the promoter of *PIEZO2*, a mechanosensitive ion channel known for contributing to sensory neuron functions [51]; *OXT, a* neuropeptide that suppresses action potential firing of DRG neurons [22; 57]; *GLRA3*, a subunit of the glycine receptor; and *TACR1*, a substance P receptor. The promoter of SP1 had binding sites on *TRPV2*, inflammation-related genes such as *TRAF1/4*, *STAT4* and *IKBKG*, and heat shock proteins like *HSF1*. Finally, SP4 showed open chromatin binding sites in Ca^{2+}-signaling-related genes such as *CACNA1G* and *CARHSP1*, as well as the interferon regulatory transcription factor, *IRF6*. Examples of genes predicted to be regulated by binding of EGR and/or SP transcription factors are depicted in **Fig. 3C**. AP-1 transcription factor and JDP2 binding

sites in males had diverse common targets in the accessible chromatin in hDRG, mainly in cytokine-related genes including *OSMR*, *IFI16*, *CCR7*, *NLRP3*, *TLR4* and *CASP8*. AP1 transcription factor binding sites were also found in GABAergic genes including *GABRA2* and *GABRB2* (**Fig. 3D**). Together, these results suggest that females and males have different transcriptional activation programs which could come play an important role in sex differences in response to injury.

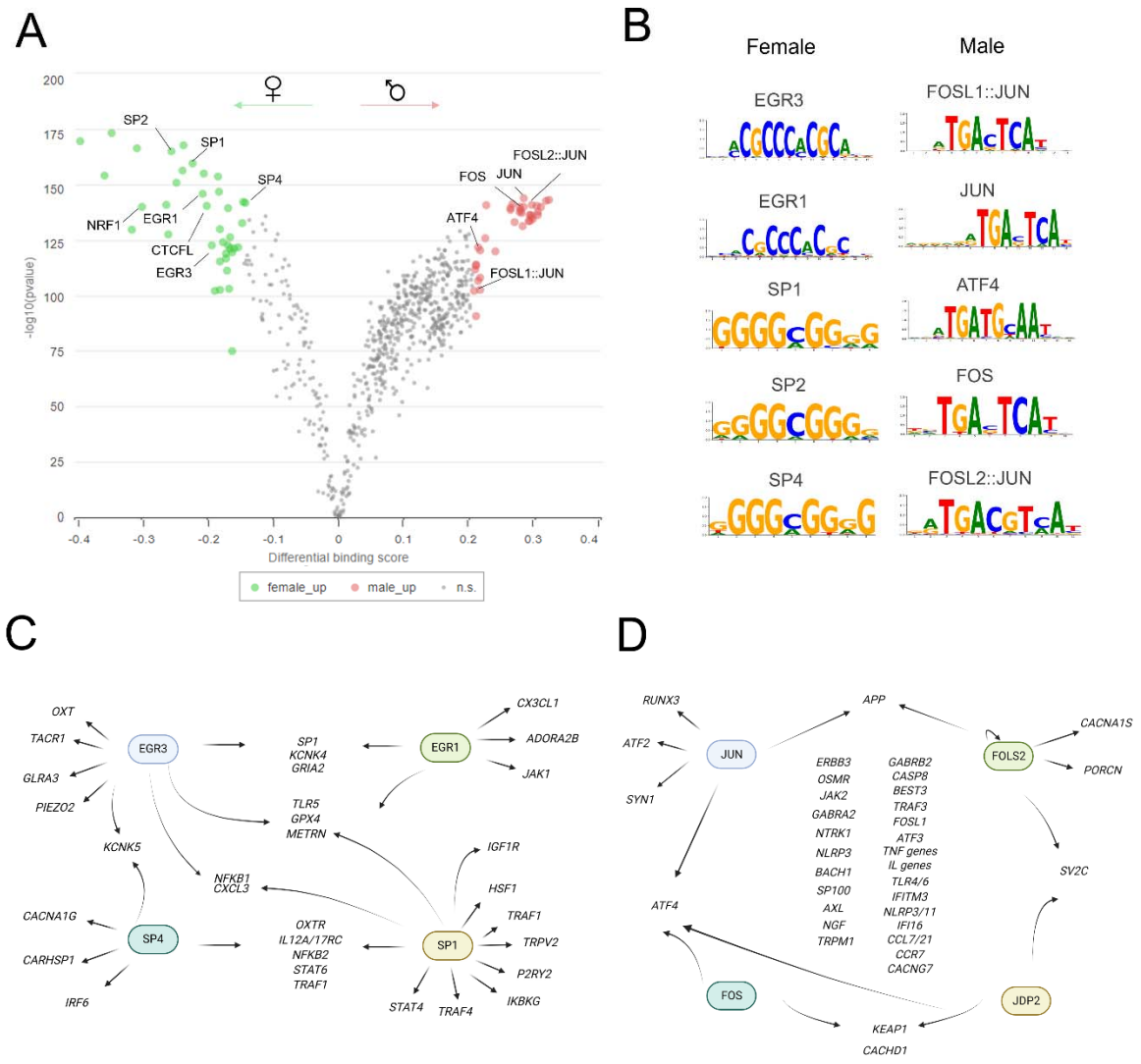

Figure 3. *Sex differences in transcription factor binding motifs within ATAC-seq peaks.* **A)** Volcano plot showing the differential transcription factor footprints enriched in female

and male hDRG identified with BINDetect (N = 9, 5 female and 4 male postmortem hDRGs, -log10 (p-value)> 95th percentiles). **B)** Differential transcription factor consensus footprints in female and male hDRG defined by reference motif on JASPAR repository. **C**) Genes predicted to bind EGR/SP factors due to transcription factor footprints in their promoters determined with TOBIAS. **D**) Genes with transcription factor binding sites for AP-1 factors in their promoters identified with TOBIAS.

Spatial ATAC-seq in hDRG

Since we did not perform neuronal selection for our bulk ATAC-seq experiments in hDRG, and spatial information is lost during dissociation, we used spatial ATAC-seq to dissect the chromatin profile in neuronal barcodes in a similar fashion to how we have done previously in spatial RNA-seq [76]. Spatial ATAC-seq was performed in hDRG tissue sections from 8 donors (N = 5 male, N =3 female) using a microfluidic barcoding system, followed by next generation sequencing [13].

We obtained 45,836 fragments on average in hDRG tissue, a TSSe score of 5.426 and a FRiP of 0.1276 of fragments of reads in peaks (**Table S6**). The improved TSS score may be due to tissue preparation, since DRGs for spatial experiments were immediately frozen in the operating room while DRGs for bulk ATAC-seq experiments were transported for 30-60 min in cold artificial cerebral spinal fluid (aCSF) prior to nuclear isolation and subsequent tagmentation (see **methods**). The average proportion of mitochondrial fragments was 4.15% (**Table S7**), and these reads were removed from the analysis. ATAC-seq fragment size distribution showed a typical periodicity of ~200 bp corresponding to reads, consistent with the length of DNA protected by mono-, di-nucleosomes (200, or 400 bp), as well as nucleosome free DNA (<100 bp) or open chromatin regions (**Fig. S1**), all of which is consistent with typical nucleosome packing [7].

In addition to neurons, there are at least 8 broadly defined cell types in hDRG [6; 30; 49]. This high hDRG cellular heterogeneity was also observed at the epigenomic level, since unsupervised cell clustering in spatial ATAC-seq samples identified 9 groups of cells (**Fig. 4A**). Cluster 1 was classified as a neuronal cluster due to the abundance of chromatin accessibility in *SNAP25* gene compared to other cell types. Further, this

cluster also shows chromatin activity for *CALCA* and *SCN10A* consistent with a neuronal phenotype (**Fig. 4B-D**). Cluster 2 showed enriched chromatin accessibility for the marker of satellite glial cells (SGCs), *FABP7* (**Fig. 4E**). The chromatin accessibility profile for cluster 3 had *CD300LB, IFI30*, *C5AR1*, *C1QB* and *ABI3* among the top 30 most active genes, all of which are expressed by immune cells in the hDRG ([6] **Fig. 4F**). According to the hDRG harmonized atlas [6], the top 30 most active genes for the cluster 5 exhibited enrichment for immune-related genes, such as *OLR1*, *MS4A7*, *TYROBP* and *CORO1A*. Interestingly, this cluster also showed enrichment for macrophage markers such as *CD163, ARHGAP30, SIRPB2* and *PLCB2*. Thus, we classified cluster 5 as immune macrophage enriched (**Fig. 4G**). Cluster 6 showed enriched chromatin accessibility in *SCN7A* likely representing the non-myelinating Schwann cell cluster (**Fig. 4H**). Cluster 7 showed enriched chromatin accessibility in *PRX* and *MPZ* representing the myelinating Schwann cell cluster (**Fig. 4I**) A fibroblast cluster was identified by the gene activity of *DCN* and *FMOD* in cluster 8 (**Fig. 4J**). Cluster 9 was identified as the endothelial cluster due to abundant *CLDN5* gene accessibility (**Fig. 4K**). Cluster 4 was more challenging to classify. This cluster showed chromatin accessibility in genes such as *PODN* and *FOXD1*, all of which are expressed in fibroblasts in hDRG suggesting this cluster is composed of a subtype of fibroblast in the hDRG. Cell type composition in hDRG section shows consistent cluster proportion between samples and sexes (**Fig. 4L**). The number of unique fragments per barcode exceeded the minimum values required to be considered high quality in all the clusters ($\log_{10}$ nFrag = 3, **Fig. 4M**). TSSe scores values per cluster and nucleosome ratio are depicted in **Fig. S2**. The number of final peaks identified across all donors was 303,850 and the genomic annotation proportion was higher in intron and distal peaks, similar to our bulk ATAC-seq experiments (**Fig. 4N**).

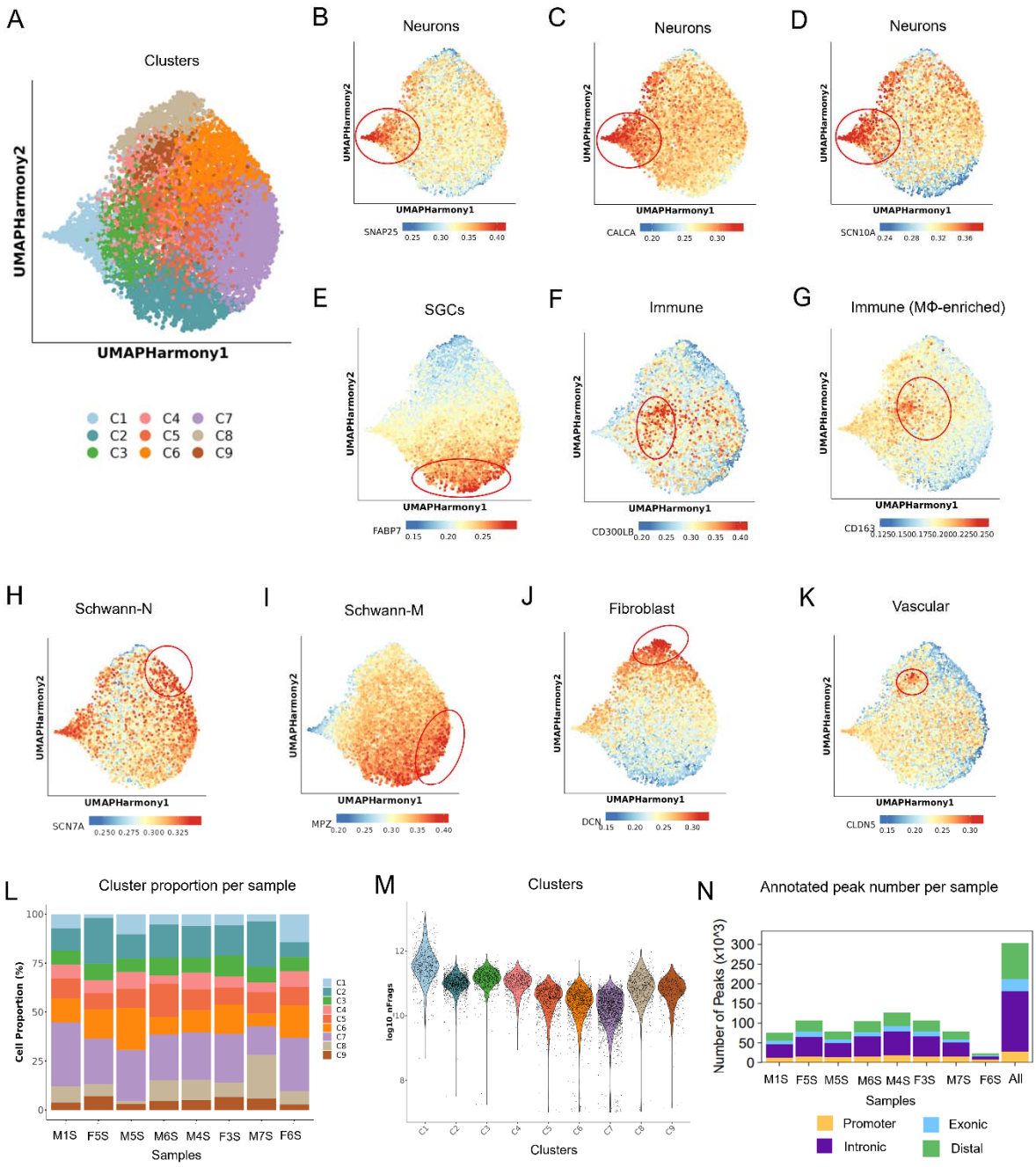

Figure 4. *Characteristics of spatial ATAC-seq in hDRG*. **A**) UMAP plot showing the 9 clusters generated by Seurat's workflow. **B-D**) UMAP plots of the chromatin accessibility of gene markers that were used to label the neuronal cluster. **E-K**) UMAP plot showing cellular populations other than neurons, including satellite glial cells (**E**), immune cells (**F**), immune cells enriched in macrophages (**G**), Schwann-N cells (**H**), Schwann-M cells

(**I**), fibroblasts (**J**) and vascular cells (**K**). **L**) Consistent cluster proportion in each sample. **M**) Violin plot shows number of unique fragments per cluster. **N**) Number of peaks identified across all donors (all), and within samples associated and their genomic annotations: promoter, intron, exon and intergenic (N = 3 female, N =5 male; samples M5S, M6S, M7S and F6S belonged to donors whose samples had not been used before for bulk ATAC-seq. A frozen hDRG sample from donors M1, M4, F3 and F5 were used for spatial ATAC-seq, and are labeled as M1S, M4S, F3S and F5S).

Pseudo-bulk analysis of spatial ATAC-seq data

We conducted a pseudo-bulk differential analysis between sexes using the reads from all the clusters in spatial ATAC-seq to have a general overview of sex differences in hDRG chromatin accessibility, which we hypothesized would be similar to our bulk ATAC-seq data (**Fig. 5**). In **figure 5A** we show that the number of fragments per barcode and the distribution of reads in the UMAP were similar between female and male hDRG samples (**Fig. 5B**). Our analysis showed DARs in 3796 genes in female hDRG versus 3827 genes in males (**Fig. 5C**). In females, a significant proportion of DARs was located on the X chromosome consistent with our bulk ATAC-seq findings (**Fig. 5D**). These findings align with our bulk ATAC-seq results. Genes such as *NONO*, *MAPD7*, *FRMPD4*, *PORCN*, *FGF13* and *TKTL1* shown in female bulk ATAC-seq were also found to be differentially accessible in female spatial ATAC-seq data. Spatial ATAC-seq also revealed female DARs in genes outside the X chromosome such as *ERBB4*, GABAergic genes including *GABRG1/2*, *GABRA5*, *GABRB3*, *GABRB1*, *GABRA2/4*, and other neuronal genes such as *BDNF*, *RELN*, *SCN9A*, *GRIA4* and *GRIN2B* (**Dataset S3**). It is important to mention that most of these genes are also significantly differentially accessible when only autosomes are analyzed, which validates our results (data not shown).

On the other hand, in males, the peaks spanned the whole genome, with a higher abundance of DARs in genes located on chromosomes 17 and 19 (**Fig. 5E**). Furthermore, a considerable amount of the genes with DARs in promoters in our bulk ATAC-seq data were also found to be biased towards males in the spatial ATAC-seq. We found male hDRG DAR-associated genes such as *FOS*, *FOSL2*, *NR1D1*, *IRF2* and

FOXO1. Male hDRG DAR list also included genes encoding for cation channels such as *TRPV2/4*. Interestingly, the male hDRG DAR list also included circadian related genes such as *BHLHE40* and *CSNK1D,* cytokines such as *CSF1R*, *CCL2*, *IL4/6R*, and alarmins *HMGA1*. Hormonal associated genes such as *INSR* and *THRA* were also found to be epigenetically more active in males. Finally, genes encoding for epigenetic remodelers such as *DOT1L*, *HDAC4*, *JARID2* and *ARID5B* were found in male hDRG.

Transcription factor (TF) motif enrichment analysis allowed us to infer differential binding sites in spatial ATAC-seq data. In females, transcription factors such as TEAD1/4, NR3C1, AR and PGR were enriched in the spatial ATAC-seq dataset. In males, peaks in DARs again belonged to the AP-1 family such as FOSB, or AP-1 interacting factor like BACH1/2 (**Fig. 5F**).

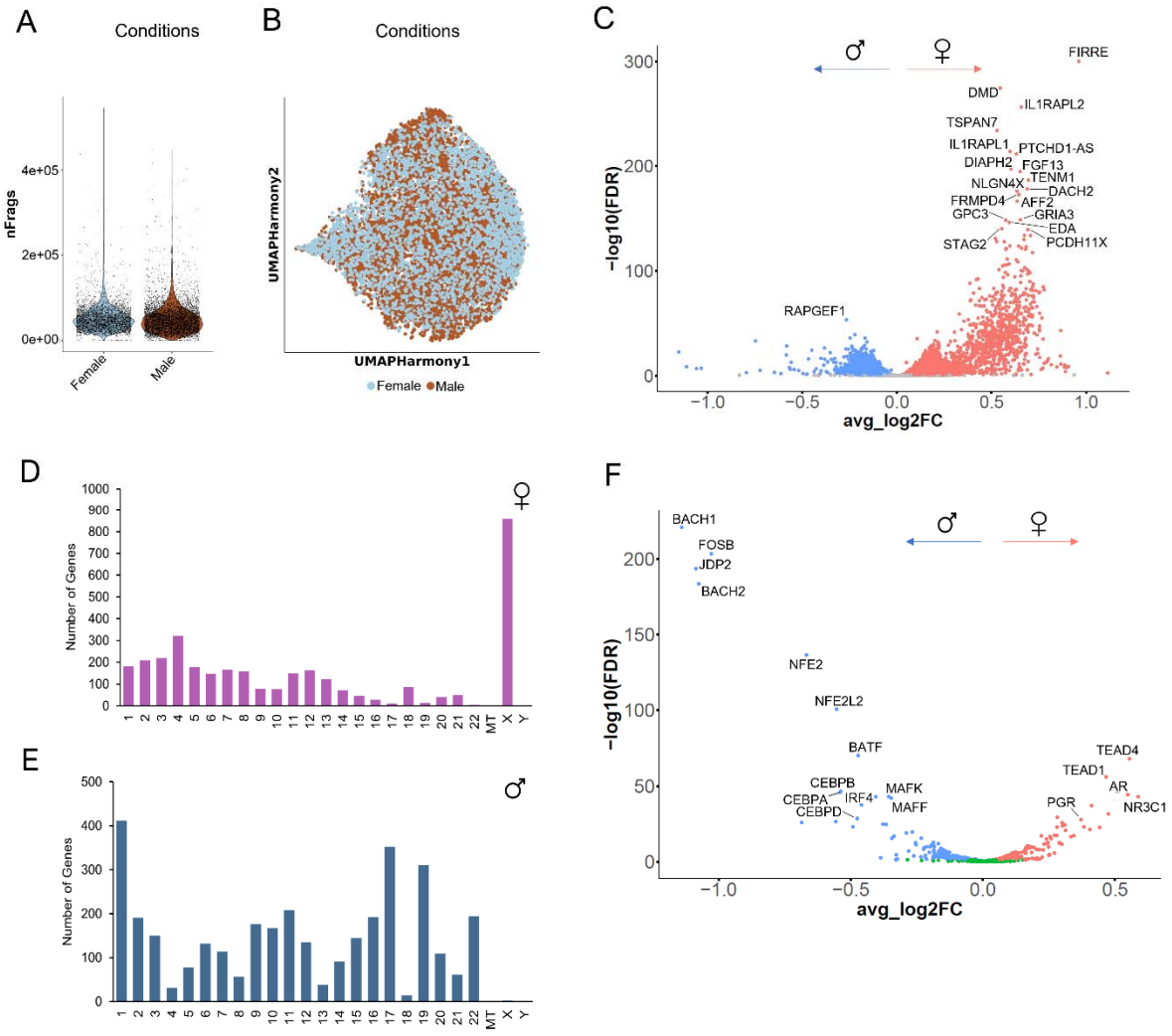

Fig. 5. *Differential spatial ATAC-seq signal in hDRG between sexes*. Analysis of sex differences in chromatin gene activity in hDRG. **A**) Number of fragments per barcode in female and male hDRG samples. **B**) UMAP of female and male barcodes distribution along hDRG cellular populations. **C**) Volcano plot showing differential ATAC-seq gene activity in a pseudo-bulk fashion in hDRG in female vs male (N = 4 female, 5 male postmortem hDRGs), FDR < 0.01 identified with ArchR. **D**) Genome location of DARs in female spatial ATAC-seq spanning the human chromosomes generated with ShinyGO. **E**) Genomic position of DARs in male hDRG. **F**) Volcano plot showing differential transcription factor binding sites in female vs male hDRG (N = 4 female, 5 male postmortem hDRGs), FDR < 0.01 identified with ArchR.

Sex differences in chromatin accessibility in hDRG neurons determined with spatial ATAC-seq

A primary motivation of our spatial ATAC-seq approach was to identify potential sex differences in neurons in hDRG. To examine this, we compared chromatin accessibility in the neuronal-enriched cluster between sexes (**Fig. 6**). DESeq2 analysis revealed DARs associated with 1665 genes in females and 1089 genes in males ($p_{adj} < 0.01$, **Fig. 6A, Dataset S4**). Similar to what we observed previously with bulk ATAC-seq or the pseudo-bulk analysis of spatial ATAC-seq data, most of the peaks in females were located on the X chromosome ($p_{adj} < 0.01$, 643 out of 1665 genes, **Fig. 6B**). In male neurons, the genes were distributed across the entire genome, and again, there was a higher abundance observed on chromosome 17 and 19 (**Fig. 6C**).

The analysis of gene ontology of genes associated to DARs between sexes showed that glutamatergic genes such as *GRIA2* and *GRIA4* to be found in the top 100 DARs in female hDRG chromatin. GABAergic genes such as *GABRB1*, *GABRG1*, *GABRE*, *GABRQ*, *GABRA1/2/3/6* were also DARs in female hDRG within the differential female gene-set, together with the lncRNA *BDNF-AS*. Enrichment analysis of accessible regions showed an association between open chromatin regions and glutamate receptor activity as the main gene ontology enriched molecular function category (pval: 0.00001581, **Fig. 6D**) determined with EnrichR [32]. Interestingly, neurons in female donors also showed DARs in *ACE2*, some interferon related genes such as *IFNB1*, *IFNA5*, *IFIH1*, *IFI44* and *CASP4*, and centromere genes such as *CENPE/W* compared to males.

In male neurons, genes such as *GRIK3* and *PTPRS* were found among DARs compared to female. Further, voltage-gated Ca^{2+} channel related genes such as *CACNA1G, CACNA1I* and *CACNA2D2* were found in the male DAR gene set. Interestingly, *TRPV3* was also a DAR in males compared to female neurons. Gene ontology analysis of the male DAR gene set revealed high abundance of calcium channel activity in the molecular function category ($p_{val} = 0.00165$, **Fig. 6E**).

Finally, we analyzed the neuronal cluster for enrichment of transcription factor binding sites in the DARs between females and males. In females, *EGR1*, *TEAD1/3/4*, *NR3C1,*

AR and *PGR* were enriched, and factors of the AP-1 family including *JUN* and *FOSB* as well as, *BACH1/2* and *IRF4* were found enriched in males (**Fig. 6F**).

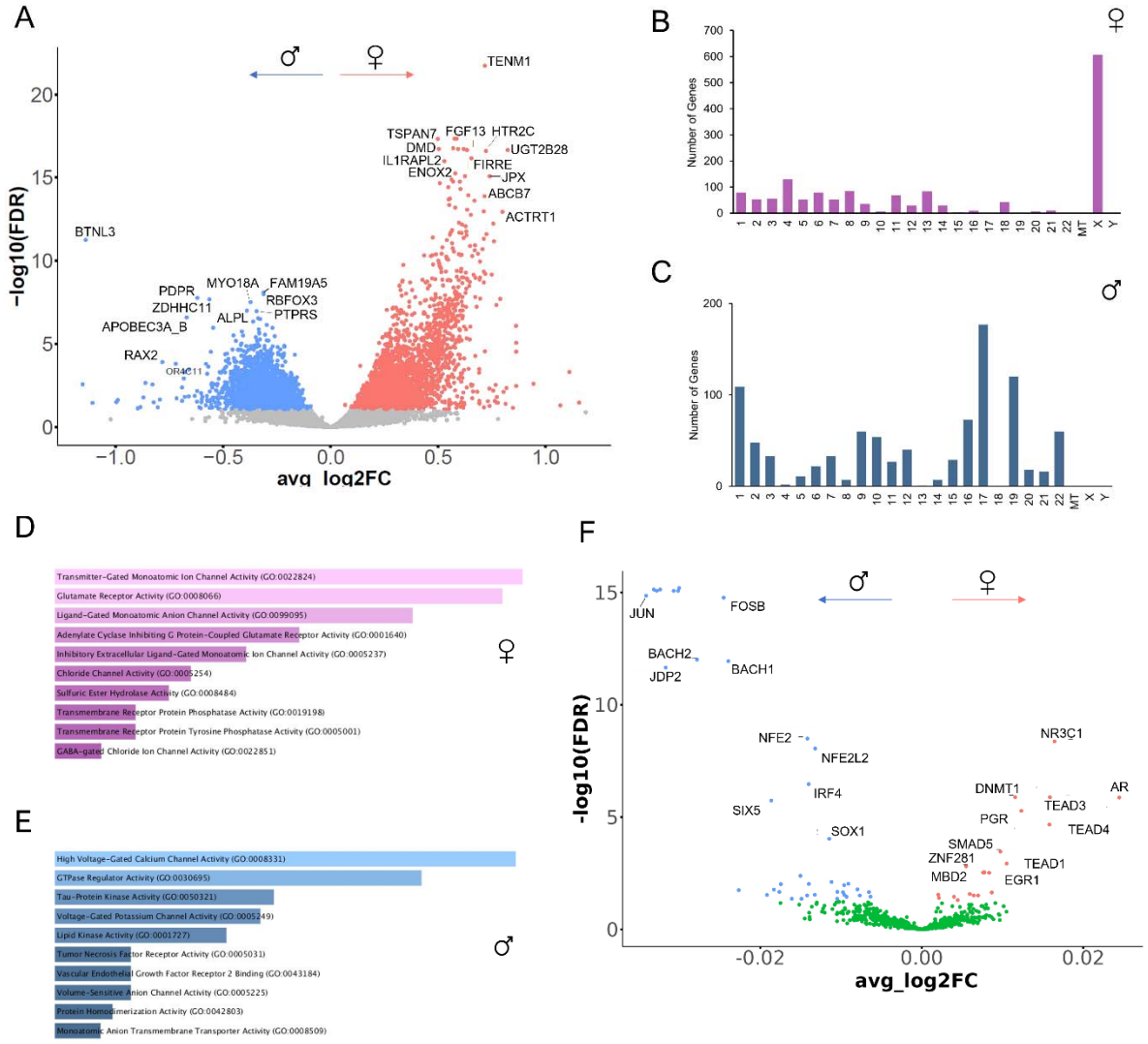

Fig. 6. *Sex differences in spatial ATAC-seq DARs in the neuronal cluster*. **A**) Volcano plot showing DARs in spatial ATAC-seq neuronal clusters in hDRG neurons in female vs male (N = 4 female, 5 male postmortem hDRGs, FDR < 0.01 identified with ArchR. **B**) Genome location of DARs in female neuronal ATAC-seq spanning the human chromosomes generated with ShinyGO. **C**) Genomic position of the DAR gene set in males. **D**) Overview of the molecular function gene ontology for DAR-associated genes in female neurons in hDRG. **E**) Summary of the gene ontology related to molecular

functions for DAR-associated genes in male neurons in hDRG. **F**) Volcano plot showing transcription factor binding site enrichment in DARs in hDRG neurons in females vs males (N = 4 female, 5 male hDRGs), FDR < 0.01 identified with ArchR.

***EGR1* expression in hDRG**

One of the outcomes that showed consistency in bulk and spatial ATAC-seq was the bias toward female in the footprint scores for the transcription factor EGR1 in hDRG, and specifically in neurons. With the aim of validating this consistent finding we sought to assess the expression of *EGR1* in hDRG using *in situ* hybridization. We found that *EGR1* is expressed in female and male hDRG *SCN10A* (+) and (-) neurons, but also in cells surrounding neurons, likely satellite glial or immune cells (**Fig. 7A-B**). We quantified the number of *EGR1* mRNAs localized to hDRG neurons and found it to be more abundant in female compared to male (**Fig. 7C**). This sexual dimorphism was statistically significant in *SCN10A* (+), but not *SCN10A* (-) cells in females (**Fig. 7D-E**). Our analysis also showed that females have a higher number of *EGR1* (+) *SCN10A* (+) cells compared to males (57.9% vs 29.71%, respectively, **Fig. 7F**). These results are consistent with our data sets. The combined identification of *EGR1* female-biased expression and the prominent abundance of regulatory binding sites in female hDRG, renders the transcriptional activity of *EGR1* a strong candidate for a female-biased regulator of gene expression in hDRG neurons.

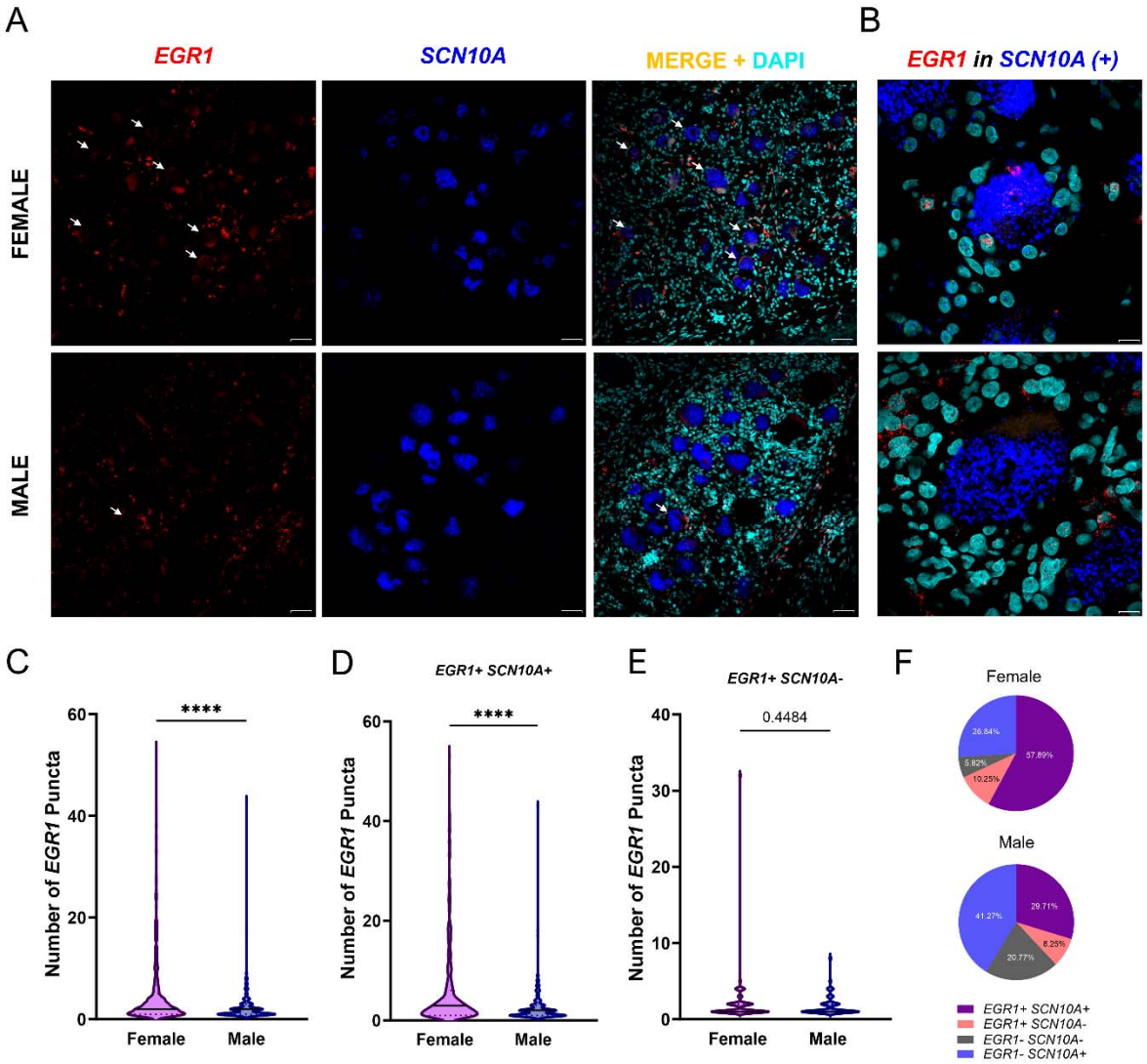

Fig. 7. *EGR1* is expressed in more *SCN10A* positive neurons in females compared to males in hDRG. **A)**. Representative *in situ* hybridization images of *EGR1* (red) in *SCN10A* (+) neurons (blue) in female and male hDRG. *EGR1* positive neurons are indicated with an arrow. **B**) 100 X magnification of neurons with *EGR1* mRNAs in female and male neurons. **C**) Total number of *EGR1* mRNAs in neurons. **D-E)** Number of *EGR1* mRNAs in *SCN10A* positive and negative neurons, respectively. **F)** Percentage of *EGR1* positive cells in *SCN10A* positive or negative cells across female and male donors in hDRG. A total of 722 neurons were analyzed to assess *EGR1* expression in female hDRG, and 727 in males (N = 5 female, N = 5 male DRG). Data

are presented as violin plots with thick line indicating the median and the dotted lines indicating the quartiles. Section thickness – 20 µm. Scale bar – 50 µm for **A** and 10 µm for **B**. ****p<0.0001 as determined by t test in **C-E**.

Patterns of chromatin accessibility in hDRG are moderately positively correlated to the transcriptomic profile.

In light of the sex dimorphic differences in chromatin accessibility between sexes in our bulk ATAC-seq results, we conducted a differential gene expression analysis on bulk nuclear RNA-seq (nucRNA-seq). RNA extractions and sequencing was performed in nuclei extracted from DRGs of 7 donors (N=3 females, N=4 males (same set of donors as in bulk ATAC-seq; details in **Table S1**). We found 8 genes that were statistically different between sexes in the nuclear compartment (p_{adj}<0.05, fold change >1.33, **Dataset S5**). Females showed higher expression of chemokine genes such as *CCL3* and *CCL4*. As expected, we found *XIST* to be differentially expressed compared to male. An interesting point to highlight is that *EGR1* and *EGR3* were trending to be highly expressed in females compared to males in our RNA-seq data (**Fig. S3A**), which aligns well with transcription factor footprints in ATAC-seq data sets and in situ hybridization experiments. On the other hand, males showed higher gene expression of non-coding genes such as *KDM5DP1*.

We tested the correlation between the log2 fold change in DARs situated in promoter and within gene bodies [23], including exon, and intron regions in ATAC-seq and the log2 fold change in nucRNA-seq for those genes in the matched hDRG samples. We found a weak positive correlation between the transcriptional and the chromatin accessibility profiling (**Fig. S3B**). This weak correlation could be explained by the repertoire of RNAs analyzed, which were limited to nuclear space and not to the whole cell. Evidence has shown that nuclear compartment harbors abundant lncRNAs and small nucleolar RNAs in human brain tissue, consistent with the expressed genes in our nucRNA-seq data, while the cytoplasm contains RNAs associated to cellular function such as metabolism, translation and protein organization compared to the nuclear compartment [90]. In addition to the small sample size, another explanation is that a high correlation was not observed since accessible regions are not necessarily

associated with actively transcribed genes, or they are associated with genes that are poised to become active under specific conditions [70]. It is important to denote that transitions in the deposition of histone modifications as well as transcription factor binding to regulatory sites such as enhancers can precede gene expression changes, inducing poised or primed chromatin states [28], which are indistinguishable from active chromatin in ATAC-seq due to a lack of epigenomic context. Further research combining different histone and DNA modifications is required to better understand the epigenomic landscape and to get a better interpretation of gene regulation in this complex tissue.

***XIST* nuclear dispersion in female hDRG neurons**

Both ATAC-seq datasets showed high accessibility for many X chromosome genes selectively in females, suggesting incomplete inactivation of the X chromosome in human, female DRG cells [1]. We explored the expression and localization of XIST RNA in hDRG because the RNA controls X inactivation to achieve gene dosage compensation between sexes by coating and inactivating one X chromosome in females [56; 61]. Although *XIST* is generally considered an exclusive long non-coding RNA in females, *XIST* has been shown to be lowly expressed in male nerve tissue [63]. We performed *in situ* hybridization for *XIST* in female and male hDRG. In females, *XIST* was expressed in neuronal and non-neuronal cells (**Fig. 8A**). Strikingly, we observed that *XIST* signal was not confined to a single area inside the neuronal nuclei. Instead, *XIST* signal was dispersed covering most of the nuclear compartment (**Fig. 8B**). This phenomenon was observed in *SCN10A*(+) and *SCN10A*(-) cells, where X spanned around 80% of the nuclear space. This observation was different in the cells surrounding the neurons, where *XIST* signal was more confined, being restricted to around 20% of the nuclear space (**Fig. 8C**). Compared to females, *XIST* was barely detected in male hDRG (**Fig. S4**). Since dispersion of XIST RNA in the nucleus is associated with incomplete X inactivation [74], these finds support the conclusion that hDRG neurons in females have incomplete X inactivation, consistent with our ATAC-seq findings.

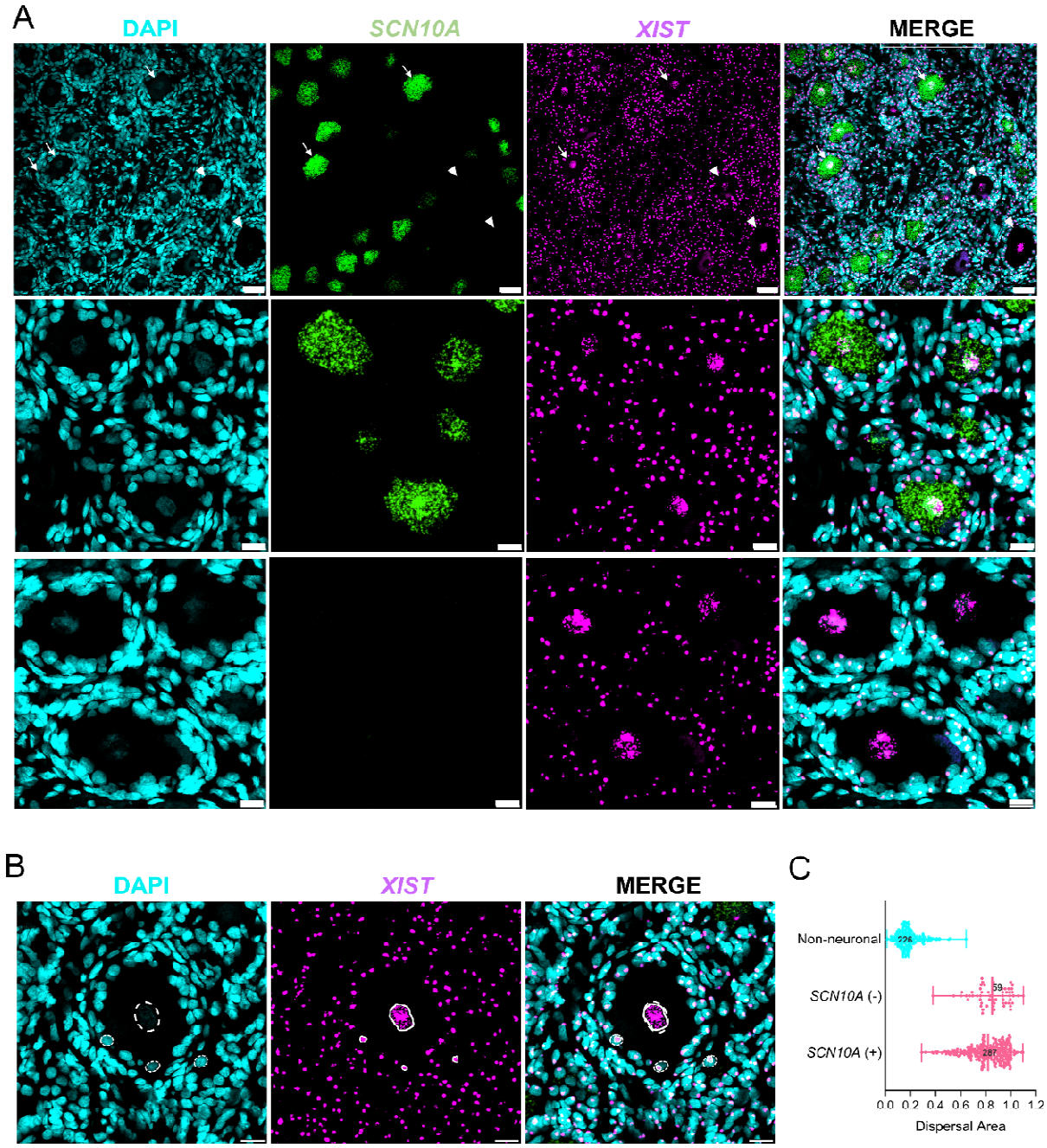

Fig. 8. *XIST* is highly dispersed in the nuclear compartment of female neurons in hDRG. **A)**. Representative *in situ* hybridization images of *XIST* (pink) in *SCN10A* (+) and *SCN10A* (-) neurons (green) in female hDRG (20X images (top), and 3X zoom magnification (bottom)). *XIST* positive neurons, also positive for *SCN10A*, are indicated with an arrow. *XIST* positive neurons, negative for *SCN10A*, are indicated with an

arrowhead. **B**) Representation of *XIST* dispersal analysis; an ROI was drawn around the nuclear compartment of neurons and non-neuronal cells (white). To delineate XIST area dispersion we drew an ROI with the dots that were furthest apart from each other (yellow). **C**) Representation of *XIST* dispersal area in *SCN10A* positive and negative neurons, and non-neuronal cells. A total of 346 neurons were analyzed to assess *XIST* expression and 226 non-neuronal cells in in female hDRG (N = 3 female, N = 2 male hDRG). Data are presented as scatter plots with lines indicating the mean and quartiles. Section thickness – 10 µm. Scale bar – 50 µm for **A** top and 20 µm for **A** bottom, and 20 µm for **B**.

Discussion

Our work provides a comprehensive view of the chromatin accessibility profile in hDRG and focuses on sex differences in tissues recovered from organ donors without any history of chronic pain or neuropathy. Chromatin structure plays a crucial role in transcription through the controlled access of regulatory factors to DNA. We mapped the accessible DNA in hDRG using two different approaches, bulk and spatial ATAC-seq. The latter approach resolved hDRG chromatin accessible profiles in distinct cell types where we focused on neuronal signatures. First, our work shows a sexual dimorphism at the chromatin level between sexes in hDRG. This dimorphism is largely influenced by the X chromosome in female hDRG suggesting a reduced X inactivation or a dormant transcriptional state that can readily become activated under certain circumstances. Second, our ATAC-seq data show a sex dimorphic signature in transcription factor bindings sites in accessible chromatin. EGR and SP motifs were more prominent in female hDRG, while AP-1 and IRF were more abundant in males. Finally, our work shows sex differences in neuronal chromatin using spatial ATAC-seq. In neurons, sex differences were partly driven by the X chromosome in females but using this approach we also uncovered differences in autosomal genes. GABA-A channels and glutamatergic genes were the molecular ontologies associated with accessible DNA in females, while voltage gated Ca^{2+} and K^{+} channel genes as well as GTP associated proteins were associated to male hDRG open chromatin.

Our bulk ATAC-seq findings point to a high chromatin accessibility in the X chromosome in females. Independently, spatial ATAC-seq confirmed this finding. It is known that one of the two X chromosomes in females is epigenetically silenced to compensate for the imbalance of X dosage between sexes [56]. X inactivation is triggered by the upregulation of *XIST* early in development. XIST coats one of the X chromosomes in *cis* [61; 66] inducing X heterochromatization via repressive epigenetic signatures [54]. Interestingly, a small subgroup of genes escapes inactivation and have epigenetic marks of active transcription, allowing gene expression from the inactive X (Xi) chromosome [1]. Our findings are consistent with previous observations showing tissue-specific varying levels of X inactivation in human tissues [79]. Further, we showed that *XIST* is highly expressed in females, and its chromatin accessibility is higher in the adult female DRG. In situ hybridization experiments show concordant results, with female having a higher abundance of *XIST* in hDRG, which is barely detected in males. Strikingly, *XIST* was found highly dispersed in the neuronal nuclei but not in the nuclei of surrounding cells in hDRG. This phenomenon has been observed in human pluripotent cells [14], where it has been hypothesized that *XIST* regulates autosomal genes in females. Future experiments should test the idea of a reduced coverage of XIST on the Xi and the consequence of a high *XIST* nuclear dispersal in hDRG neurons. Our results are also consistent with a recent study showing greater variability in X inactivation in excitatory neurons in the human brain suggesting enhanced expression of genes from this chromosome in women in this population of neurons that shares a glutamatergic biochemical phenotype with DRG neurons [84].

It is now recognized that sex dimorphisms in pathological conditions like autoimmune diseases, can be driven by tissue or cell-specific patterns of X-inactivation. We observed higher chromatin accessibility mainly in genes coding for GABA-A receptor subunits, glutamatergic and interferon-related genes in females, some of which are located in X chromosome. This is in line with previous findings showing that interferon-related genes are more highly expressed in female hDRG from neuropathic pain patients undergoing thoracic vertebrectomy surgery [59]. *ACE2,* an interferon stimulated gene located in the X chromosome, is expressed in hDRG neurons, serving as potential entry site for SARS-CoV-2 in the PNS [69]. Delving deeper into the study of X

inactivation escape in hDRG will shed light on the organization of chromatin in this chromosome and improve our understanding of its implications for chronic pain mechanisms in women. Importantly, a previous study linked X inactivation escape in blood cells to development of chronic pain after motor vehicle accident supporting the relevance of this line of investigation [89]. On the other hand, some of the female-biased genes were associated with DARs on autosomes, such as *GABRA5*. It has been shown that the α_5-$GABA_A$ receptor (encoded by the *Gabra5* gene in mice) is more highly expressed in the female rodent DRG where it plays an important role in pain signaling and is epigenetically regulated in a sex-specific fashion [17; 18]. We also found a higher accessibility in autosomal *BDNF-AS*, a lncRNA that suppresses *BDNF* expression. It is well-established that BDNF is released from primary afferents [33] binding to TrkB in spinal cord neurons where it regulates synaptic plasticity important for chronic pain [11]. Our findings suggest that *BDNF-AS* could be an unappreciated suppressor of BDNF expression in females, a relevant finding because the role of BDNF signaling is more prominent in male than in female rodents [38; 48] and in male but not female human spinal cord [12].

At the level of transcription factor footprints, EGR1/3 and SP showed higher abundance in female accessible DNA in hDRG. In agreement with this, *EGR1* expression was higher in females. EGR1 is a transcription factor classified as immediate early gene. EGR1-driven transcriptional programs are activated by stimuli like cytokines, growth factors, oxidative stress, hypoxia and injury [85]. Further, Egr1 has an important role in neuronal plasticity in the adult nervous system [15]. A recent study found that the expression of *Egr1* is driven by female sex hormones and acts as a chromatin modifier in a sex-specific fashion [60], suggesting its pivotal role in controlling neuronal gene expression in females. Our data shows that EGR1 binding sites are found in genes like *JAK1* and *CX3CL1*, both of which are interferon associated genes known to induce pain through a peripheral mechanism in mouse models [2; 19]. This is also consistent with human thoracic vertebrectomy DRG data showing that interferon and JAK-STAT signaling are associated with neuropathic pain in female samples but not in males [59]. One inconsistency with the thoracic vertebrectomy data is that *EGR1* mRNA was more highly expressed in males with pain than females [59], but the impact of that difference

likely depends on access to regulatory sites for the transcription factor. Also consistent with our findings, *SP4* has a higher expression in female tibial nerve compared to male [58]. SP4 regulates the transcription of pain-related genes [9] and, Sp4 knockdown reverses the hypersensitivity induced by persistent models of pain in mice, suggesting an important role of this transcription factor to pain [67]. Binding sites of other members of the SP (*SP1*/*SP5*) family were abundant in accessible chromatin in female hDRG, rendering these transcription factors potential therapeutic targets for treating pain in females since they are linked to neuropathies such as of chemotherapy-induced peripheral neuropathy [86].

In males, we observed a higher chromatin accessibility in *TRPV2/4* and Ca^{2+}-related genes in hDRG, with the latter specifically in neurons. With respect to the former group of genes, many of these play important roles in pain but *TRPV4* is the only TRP channel that shows higher expression in pain samples from thoracic vertebrectomy pain patients in males versus females [59]. While we are not aware of any previous reports of sex differences in expression of Ca^{2+}-related genes in hDRG, rodent studies demonstrate that some calcium-related genes including *Cacna1b* are upregulated in male DRG in a model of nerve injury, gene that showed higher accessibility in male hDRG in our data [71]. At the level of transcriptional programs, AP-1 transcription factors were predominant in male hDRG in both bulk and spatial ATAC-seq specifically in neurons. These data are in close agreement with increased JUN and FOS activated transcriptional cascades in DRGs from male patients with neuropathic pain in the thoracic vertebrectomy cohort [59]. We found that the promoters of genes such as *OSMR*, *NLRP3* or *CASP8* are predicted to be bound by these transcription factors. The abundance of binding sites for these genes in male open chromatin in the DRG increases the likelihood that they will be activated under conditions of inflammation or injury, which is consistent with the findings of the thoracic vertebrectomy cohort where OSM signaling was specifically upregulated in males [50; 59].

Collectively, our data demonstrate distinct baseline sex-specific chromatin accessibility patterns and transcriptional programs primed for activation by injury or inflammation in hDRG. Functional differences observed in female hDRG, such as increased

accessibility of GABAergic, glutamatergic and interferon-related genes, could contribute to their heightened susceptibility to chronic pain. Conversely, higher accessibility of calcium signaling genes in males might underlie distinct pain mechanisms. These findings highlight the importance of considering sex as a biological variable in chronic pain research and potentially pave the way for the development of sex-specific therapeutic strategies.

Limitations

One important limitation of our work is that we did not perform multi-ome analysis from the same cell, making it difficult to test for direct correlation of gene expression and chromatin accessibility. Further, our sample size is relatively small. This can be improved with additional studies, which should include samples from individuals with chronic pain. We note, however, that we could achieve our primary objective of detecting sex differences, many of which were replicated with two independent methods. Additional experiments like CUT&Tag sequencing [29] can be used to gain insight into the epigenetic landscape in the hDRG. Our work with organ donor DRGs shows that tissue quality is sufficient to enable these future studies.

Conflict of Interest Statement

The authors declare no financial conflicts of interest related to this work.

Acknowledgements

We acknowledge Yeunhee Kim, Manager of Genome Center at the University of Texas at Dallas for technical support with library prep for sequencing. We acknowledge Jennifer Garbarino, Andrés Hernández-Oliveras, Abhira Ravirala and Zawge Yohannes Daniel for the technical support to this project. The authors thank Anna Cervantes, Geoffrey Funk, and Peter Horton at the Southwest Transplant Alliance. The authors are grateful to the organ donors and their families for their gift. Data availability: Data in this paper will be uploaded to SPARC Portal. This work was supported by the National Institutes of Health grant U19NS130608 and R01NS111929 to Theodore J. Price.

References

[1] Balaton BP, Brown CJ. Escape Artists of the X Chromosome. Trends Genet 2016;32(6):348-359.

[2] Barragan-Iglesias P, Kuhn J, Vidal-Cantu GC, Salinas-Abarca AB, Granados-Soto V, Dussor GO, Campbell ZT, Price TJ. Activation of the integrated stress response in nociceptors drives methylglyoxal-induced pain. Pain 2019;160(1):160-171.

[3] Barter MJ, Cheung K, Falk J, Panagiotopoulos AC, Cosimini C, O'Brien S, Teja-Putri K, Neill G, Deehan DJ, Young DA. Dynamic chromatin accessibility landscape changes following interleukin-1 stimulation. Epigenetics 2021;16(1):106-119.

[4] Bentsen M, Goymann P, Schultheis H, Klee K, Petrova A, Wiegandt R, Fust A, Preussner J, Kuenne C, Braun T, Kim J, Looso M. ATAC-seq footprinting unravels kinetics of transcription factor binding during zygotic genome activation. Nat Commun 2020;11(1):4267.

[5] Berkley KJ. Sex differences in pain. Behav Brain Sci 1997;20(3):371-380; discussion 435-513.

[6] Bhuiyan SA, Xu M, Yang L, Semizoglou E, Bhatia P, Pantaleo KI, Tochitsky I, Jain A, Erdogan B, Blair S, Cat V, Mwirigi JM, Sankaranarayanan I, Tavares-Ferreira D, Green U, McIlvried LA, Copits BA, Bertels Z, Del Rosario JS, Widman AJ, Slivicki RA, Yi J, Woolf CJ, Lennerz JK, Whited JL, Price TJ, Gereau RW, Renthal W. Harmonized cross-species cell atlases of trigeminal and dorsal root ganglia. bioRxiv 2023.

[7] Buenrostro JD, Giresi PG, Zaba LC, Chang HY, Greenleaf WJ. Transposition of native chromatin for fast and sensitive epigenomic profiling of open chromatin, DNA-binding proteins and nucleosome position. Nat Methods 2013;10(12):1213-1218.

[8] Buenrostro JD, Wu B, Chang HY, Greenleaf WJ. ATAC-seq: A Method for Assaying Chromatin Accessibility Genome-Wide. Curr Protoc Mol Biol 2015;109:21 29 21-21 29 29.

[9] Chu C, Zavala K, Fahimi A, Lee J, Xue Q, Eilers H, Schumacher MA. Transcription factors Sp1 and Sp4 regulate TRPV1 gene expression in rat sensory neurons. Mol Pain 2011;7:44.

[10] Corces MR, Trevino AE, Hamilton EG, Greenside PG, Sinnott-Armstrong NA, Vesuna S, Satpathy AT, Rubin AJ, Montine KS, Wu B, Kathiria A, Cho SW, Mumbach MR, Carter AC, Kasowski M, Orloff LA, Risca VI, Kundaje A, Khavari PA, Montine TJ, Greenleaf WJ, Chang HY. An improved ATAC-seq protocol reduces background and enables interrogation of frozen tissues. Nat Methods 2017;14(10):959-962.

[11] Coull JA, Beggs S, Boudreau D, Boivin D, Tsuda M, Inoue K, Gravel C, Salter MW, De Koninck Y. BDNF from microglia causes the shift in neuronal anion gradient underlying neuropathic pain. Nature 2005;438(7070):1017-1021.

[12] Dedek A, Xu J, Lorenzo LE, Godin AG, Kandegedara CM, Glavina G, Landrigan JA, Lombroso PJ, De Koninck Y, Tsai EC, Hildebrand ME. Sexual dimorphism in a neuronal mechanism of spinal hyperexcitability across rodent and human models of pathological pain. Brain 2022;145(3):1124-1138.

[13] Deng Y, Bartosovic M, Ma S, Zhang D, Kukanja P, Xiao Y, Su G, Liu Y, Qin X, Rosoklija GB, Dwork AJ, Mann JJ, Xu ML, Halene S, Craft JE, Leong KW, Boldrini M, Castelo-Branco G, Fan R. Spatial profiling of chromatin accessibility in mouse and human tissues. Nature 2022;609(7926):375-383.

[14] Dror I, Chitiashvili T, Tan SYX, Cano CT, Sahakyan A, Markaki Y, Chronis C, Collier AJ, Deng W, Liang G, Sun Y, Afasizheva A, Miller J, Xiao W, Black DL, Ding F, Plath K. XIST directly regulates X-linked and autosomal genes in naive human pluripotent cells. Cell 2024;187(1):110-129 e131.

[15] Duclot F, Kabbaj M. The Role of Early Growth Response 1 (EGR1) in Brain Plasticity and Neuropsychiatric Disorders. Front Behav Neurosci 2017;11:35.

[16] Fillingim RB, King CD, Ribeiro-Dasilva MC, Rahim-Williams B, Riley JL, 3rd. Sex, gender, and pain: a review of recent clinical and experimental findings. J Pain 2009;10(5):447-485.

[17] Franco-Enzastiga U, De la Luz-Cuellar YE, Hernandez Reyes LE, Raya-Tafolla G, Torres-Lopez JE, Murbartian J, Granados-Soto V, Delgado-Lezama R. Extrasynaptic α5GABAA receptors and their role in nociception and pathological pain. In: R Rajendram, VR Preedy, V Patel, CR Martin, editors. The Neurobiology, Physiology, and Psychology of Pain: Academic Press, 2022. pp. 129-137.
[18] Franco-Enzastiga U, Garcia G, Murbartian J, Gonzalez-Barrios R, Salinas-Abarca AB, Sanchez-Hernandez B, Tavares-Ferreira D, Herrera LA, Barragan-Iglesias P, Delgado-Lezama R, Price TJ, Granados-Soto V. Sex-dependent pronociceptive role of spinal alpha(5) -GABA(A) receptor and its epigenetic regulation in neuropathic rodents. J Neurochem 2021;156(6):897-916.
[19] Franco-Enzastiga U, Natarajan K, David ET, Patel K, Ravirala A, Price TJ. Vinorelbine causes a neuropathic pain-like state in mice via STING and MNK1 signaling associated with type I interferon induction. iScience 2024;27(2):108808.
[20] Ghazisaeidi S, Muley MM, Salter MW. Neuropathic Pain: Mechanisms, Sex Differences, and Potential Therapies for a Global Problem. Annu Rev Pharmacol Toxicol 2023;63:565-583.
[21] Ghosh K, Pan HL. Epigenetic Mechanisms of Neural Plasticity in Chronic Neuropathic Pain. ACS Chem Neurosci 2022;13(4):432-441.
[22] Gong L, Gao F, Li J, Li J, Yu X, Ma X, Zheng W, Cui S, Liu K, Zhang M, Kunze W, Liu CY. Oxytocin-induced membrane hyperpolarization in pain-sensitive dorsal root ganglia neurons mediated by Ca(2+)/nNOS/NO/KATP pathway. Neuroscience 2015;289:417-428.
[23] Granja JM, Corces MR, Pierce SE, Bagdatli ST, Choudhry H, Chang HY, Greenleaf WJ. ArchR is a scalable software package for integrative single-cell chromatin accessibility analysis. Nat Genet 2021;53(3):403-411.
[24] Greenspan JD, Craft RM, LeResche L, Arendt-Nielsen L, Berkley KJ, Fillingim RB, Gold MS, Holdcroft A, Lautenbacher S, Mayer EA, Mogil JS, Murphy AZ, Traub RJ, Consensus Working Group of the Sex G, Pain SIGotI. Studying sex and gender differences in pain and analgesia: a consensus report. Pain 2007;132 Suppl 1(Suppl 1):S26-S45.
[25] Gregus AM, Levine IS, Eddinger KA, Yaksh TL, Buczynski MW. Sex differences in neuroimmune and glial mechanisms of pain. Pain 2021;162(8):2186-2200.
[26] Hauberg ME, Creus-Muncunill J, Bendl J, Kozlenkov A, Zeng B, Corwin C, Chowdhury S, Kranz H, Hurd YL, Wegner M, Borglum AD, Dracheva S, Ehrlich ME, Fullard JF, Roussos P. Common schizophrenia risk variants are enriched in open chromatin regions of human glutamatergic neurons. Nat Commun 2020;11(1):5581.
[27] Huang ZZ, Li D, Liu CC, Cui Y, Zhu HQ, Zhang WW, Li YY, Xin WJ. CX3CL1-mediated macrophage activation contributed to paclitaxel-induced DRG neuronal apoptosis and painful peripheral neuropathy. Brain Behav Immun 2014;40:155-165.
[28] Ito S, Das ND, Umehara T, Koseki H. Factors and Mechanisms That Influence Chromatin-Mediated Enhancer-Promoter Interactions and Transcriptional Regulation. Cancers (Basel) 2022;14(21).
[29] Janssens DH, Greene JE, Wu SJ, Codomo CA, Minot SS, Furlan SN, Ahmad K, Henikoff S. Scalable single-cell profiling of chromatin modifications with sciCUT&Tag. Nat Protoc 2024;19(1):83-112.
[30] Jung M, Dourado M, Maksymetz J, Jacobson A, Laufer BI, Baca M, Foreman O, Hackos DH, Riol-Blanco L, Kaminker JS. Cross-species transcriptomic atlas of dorsal root ganglia reveals species-specific programs for sensory function. Nat Commun 2023;14(1):366.
[31] Klemm SL, Shipony Z, Greenleaf WJ. Chromatin accessibility and the regulatory epigenome. Nat Rev Genet 2019;20(4):207-220.
[32] Kuleshov MV, Jones MR, Rouillard AD, Fernandez NF, Duan Q, Wang Z, Koplev S, Jenkins SL, Jagodnik KM, Lachmann A, McDermott MG, Monteiro CD, Gundersen GW, Ma'ayan A. Enrichr: a comprehensive gene set enrichment analysis web server 2016 update. Nucleic Acids Res 2016;44(W1):W90-97.

[33] Latremoliere A, Woolf CJ. Central sensitization: a generator of pain hypersensitivity by central neural plasticity. J Pain 2009;10(9):895-926.
[34] Laumet G, Garriga J, Chen SR, Zhang Y, Li DP, Smith TM, Dong Y, Jelinek J, Cesaroni M, Issa JP, Pan HL. G9a is essential for epigenetic silencing of K(+) channel genes in acute-to-chronic pain transition. Nat Neurosci 2015;18(12):1746-1755.
[35] Liao J, Zhang F, Qing W, Yu R, Hu Z. Mechanism of Incisional Pain: Novel Finding on Long Noncoding RNA XIST/miR-340-5p/RAB1A Axis. ASN Neuro 2021;13:17590914211049056.
[36] Lopes DM, Malek N, Edye M, Jager SB, McMurray S, McMahon SB, Denk F. Sex differences in peripheral not central immune responses to pain-inducing injury. Sci Rep 2017;7(1):16460.
[37] Manners MT, Ertel A, Tian Y, Ajit SK. Genome-wide redistribution of MeCP2 in dorsal root ganglia after peripheral nerve injury. Epigenetics Chromatin 2016;9:23.
[38] Mapplebeck JCS, Lorenzo LE, Lee KY, Gauthier C, Muley MM, De Koninck Y, Prescott SA, Salter MW. Chloride Dysregulation through Downregulation of KCC2 Mediates Neuropathic Pain in Both Sexes. Cell Rep 2019;28(3):590-596 e594.
[39] Margueron R, Reinberg D. Chromatin structure and the inheritance of epigenetic information. Nat Rev Genet 2010;11(4):285-296.
[40] Marquez EJ, Chung CH, Marches R, Rossi RJ, Nehar-Belaid D, Eroglu A, Mellert DJ, Kuchel GA, Banchereau J, Ucar D. Sexual-dimorphism in human immune system aging. Nat Commun 2020;11(1):751.
[41] Matsushita Y, Araki K, Omotuyi O, Mukae T, Ueda H. HDAC inhibitors restore C-fibre sensitivity in experimental neuropathic pain model. Br J Pharmacol 2013;170(5):991-998.
[42] Mecklenburg J, Zou Y, Wangzhou A, Garcia D, Lai Z, Tumanov AV, Dussor G, Price TJ, Akopian AN. Transcriptomic sex differences in sensory neuronal populations of mice. Sci Rep 2020;10(1):15278.
[43] Mich JK, Graybuck LT, Hess EE, Mahoney JT, Kojima Y, Ding Y, Somasundaram S, Miller JA, Kalmbach BE, Radaelli C, Gore BB, Weed N, Omstead V, Bishaw Y, Shapovalova NV, Martinez RA, Fong O, Yao S, Mortrud M, Chong P, Loftus L, Bertagnolli D, Goldy J, Casper T, Dee N, Opitz-Araya X, Cetin A, Smith KA, Gwinn RP, Cobbs C, Ko AL, Ojemann JG, Keene CD, Silbergeld DL, Sunkin SM, Gradinaru V, Horwitz GD, Zeng H, Tasic B, Lein ES, Ting JT, Levi BP. Functional enhancer elements drive subclass-selective expression from mouse to primate neocortex. Cell Rep 2021;34(13):108754.
[44] Mine-Hattab J, Chiolo I. Complex Chromatin Motions for DNA Repair. Front Genet 2020;11:800.
[45] Mogil JS. Perspective: Equality need not be painful. Nature 2016;535(7611):S7.
[46] Mogil JS. Qualitative sex differences in pain processing: emerging evidence of a biased literature. Nat Rev Neurosci 2020;21(7):353-365.
[47] Mogil JS, Bailey AL. Sex and gender differences in pain and analgesia. Prog Brain Res 2010;186:141-157.
[48] Moy JK, Szabo-Pardi T, Tillu DV, Megat S, Pradhan G, Kume M, Asiedu MN, Burton MD, Dussor G, Price TJ. Temporal and sex differences in the role of BDNF/TrkB signaling in hyperalgesic priming in mice and rats. Neurobiol Pain 2019;5:100024.
[49] Nguyen MQ, von Buchholtz LJ, Reker AN, Ryba NJ, Davidson S. Single-nucleus transcriptomic analysis of human dorsal root ganglion neurons. Elife 2021;10.
[50] North RY, Li Y, Ray P, Rhines LD, Tatsui CE, Rao G, Johansson CA, Zhang H, Kim YH, Zhang B, Dussor G, Kim TH, Price TJ, Dougherty PM. Electrophysiological and transcriptomic correlates of neuropathic pain in human dorsal root ganglion neurons. Brain 2019;142(5):1215-1226.
[51] Obeidat AM, Wood MJ, Adamczyk NS, Ishihara S, Li J, Wang L, Ren D, Bennett DA, Miller RJ, Malfait AM, Miller RE. Piezo2 expressing nociceptors mediate mechanical sensitization in experimental osteoarthritis. Nat Commun 2023;14(1):2479.

[52] Parisien M, Khoury S, Chabot-Dore AJ, Sotocinal SG, Slade GD, Smith SB, Fillingim RB, Ohrbach R, Greenspan JD, Maixner W, Mogil JS, Belfer I, Diatchenko L. Effect of Human Genetic Variability on Gene Expression in Dorsal Root Ganglia and Association with Pain Phenotypes. Cell Rep 2017;19(9):1940-1952.
[53] Patil M, Belugin S, Mecklenburg J, Wangzhou A, Paige C, Barba-Escobedo PA, Boyd JT, Goffin V, Grattan D, Boehm U, Dussor G, Price TJ, Akopian AN. Prolactin Regulates Pain Responses via a Female-Selective Nociceptor-Specific Mechanism. iScience 2019;20:449-465.
[54] Patrat C, Ouimette JF, Rougeulle C. X chromosome inactivation in human development. Development 2020;147(1).
[55] Pieretti S, Di Giannuario A, Di Giovannandrea R, Marzoli F, Piccaro G, Minosi P, Aloisi AM. Gender differences in pain and its relief. Ann Ist Super Sanita 2016;52(2):184-189.
[56] Popova BC, Tada T, Takagi N, Brockdorff N, Nesterova TB. Attenuated spread of X-inactivation in an X;autosome translocation. Proc Natl Acad Sci U S A 2006;103(20):7706-7711.
[57] Qiu F, Qiu CY, Cai H, Liu TT, Qu ZW, Yang Z, Li JD, Zhou QY, Hu WP. Oxytocin inhibits the activity of acid-sensing ion channels through the vasopressin, V1A receptor in primary sensory neurons. Br J Pharmacol 2014;171(12):3065-3076.
[58] Ray PR, Khan J, Wangzhou A, Tavares-Ferreira D, Akopian AN, Dussor G, Price TJ. Transcriptome Analysis of the Human Tibial Nerve Identifies Sexually Dimorphic Expression of Genes Involved in Pain, Inflammation, and Neuro-Immunity. Front Mol Neurosci 2019;12:37.
[59] Ray PR, Shiers S, Caruso JP, Tavares-Ferreira D, Sankaranarayanan I, Uhelski ML, Li Y, North RY, Tatsui C, Dussor G, Burton MD, Dougherty PM, Price TJ. RNA profiling of human dorsal root ganglia reveals sex differences in mechanisms promoting neuropathic pain. Brain 2023;146(2):749-766.
[60] Rocks D, Purisic E, Gallo EF, Greally JM, Suzuki M, Kundakovic M. Egr1 is a sex-specific regulator of neuronal chromatin, synaptic plasticity, and behaviour. bioRxiv 2023.
[61] Rodermund L, Coker H, Oldenkamp R, Wei G, Bowness J, Rajkumar B, Nesterova T, Susano Pinto DM, Schermelleh L, Brockdorff N. Time-resolved structured illumination microscopy reveals key principles of Xist RNA spreading. Science 2021;372(6547).
[62] Rosen S, Ham B, Mogil JS. Sex differences in neuroimmunity and pain. J Neurosci Res 2017;95(1-2):500-508.
[63] Sadagopan A, Nasim IT, Li J, Achom M, Zhang CZ, Viswanathan SR. Somatic XIST activation and features of X chromosome inactivation in male human cancers. Cell Syst 2022;13(11):932-944 e935.
[64] San Roman AK, Skaletsky H, Godfrey AK, Bokil NV, Teitz L, Singh I, Blanton LV, Bellott DW, Pyntikova T, Lange J, Koutseva N, Hughes JF, Brown L, Phou S, Buscetta A, Kruszka P, Banks N, Dutra A, Pak E, Lasutschinkow PC, Keen C, Davis SM, Lin AE, Tartaglia NR, Samango-Sprouse C, Muenke M, Page DC. The human Y and inactive X chromosomes similarly modulate autosomal gene expression. bioRxiv 2023.
[65] Schang AL, Saberan-Djoneidi D, Mezger V. The impact of epigenomic next-generation sequencing approaches on our understanding of neuropsychiatric disorders. Clin Genet 2018;93(3):467-480.
[66] Schwammle T, Schulz EG. Regulatory principles and mechanisms governing the onset of random X-chromosome inactivation. Curr Opin Genet Dev 2023;81:102063.
[67] Sheehan K, Lee J, Chong J, Zavala K, Sharma M, Philipsen S, Maruyama T, Xu Z, Guan Z, Eilers H, Kawamata T, Schumacher M. Transcription factor Sp4 is required for hyperalgesic state persistence. PLoS One 2019;14(2):e0211349.
[68] Shenoda BB, Ramanathan S, Gupta R, Tian Y, Jean-Toussaint R, Alexander GM, Addya S, Somarowthu S, Sacan A, Ajit SK. Xist attenuates acute inflammatory response by female cells. Cell Mol Life Sci 2021;78(1):299-316.

[69] Shiers S, Ray PR, Wangzhou A, Sankaranarayanan I, Tatsui CE, Rhines LD, Li Y, Uhelski ML, Dougherty PM, Price TJ. ACE2 and SCARF expression in human dorsal root ganglion nociceptors: implications for SARS-CoV-2 virus neurological effects. Pain 2020;161(11):2494-2501.
[70] Starks RR, Biswas A, Jain A, Tuteja G. Combined analysis of dissimilar promoter accessibility and gene expression profiles identifies tissue-specific genes and actively repressed networks. Epigenetics Chromatin 2019;12(1):16.
[71] Stephens KE, Zhou W, Ji Z, Chen Z, He S, Ji H, Guan Y, Taverna SD. Sex differences in gene regulation in the dorsal root ganglion after nerve injury. BMC Genomics 2019;20(1):147.
[72] Stephens KE, Zhou W, Renfro Z, Ji Z, Ji H, Guan Y, Taverna SD. Global gene expression and chromatin accessibility of the peripheral nervous system in animal models of persistent pain. J Neuroinflammation 2021;18(1):185.
[73] Sun W, Ma M, Yu H, Yu H. Inhibition of lncRNA X inactivate-specific transcript ameliorates inflammatory pain by suppressing satellite glial cell activation and inflammation by acting as a sponge of miR-146a to inhibit Na(v) 1.7. J Cell Biochem 2018;119(12):9888-9898.
[74] Sunwoo H, Colognori D, Froberg JE, Jeon Y, Lee JT. Repeat E anchors Xist RNA to the inactive X chromosomal compartment through CDKN1A-interacting protein (CIZ1). Proc Natl Acad Sci U S A 2017;114(40):10654-10659.
[75] Tavares-Ferreira D, Ray PR, Sankaranarayanan I, Mejia GL, Wangzhou A, Shiers S, Uttarkar R, Megat S, Barragan-Iglesias P, Dussor G, Akopian AN, Price TJ. Sex Differences in Nociceptor Translatomes Contribute to Divergent Prostaglandin Signaling in Male and Female Mice. Biol Psychiatry 2022;91(1):129-140.
[76] Tavares-Ferreira D, Shiers S, Ray PR, Wangzhou A, Jeevakumar V, Sankaranarayanan I, Cervantes AM, Reese JC, Chamessian A, Copits BA, Dougherty PM, Gereau RWt, Burton MD, Dussor G, Price TJ. Spatial transcriptomics of dorsal root ganglia identifies molecular signatures of human nociceptors. Sci Transl Med 2022;14(632):eabj8186.
[77] Thibodeau A, Uyar A, Khetan S, Stitzel ML, Ucar D. A neural network based model effectively predicts enhancers from clinical ATAC-seq samples. Sci Rep 2018;8(1):16048.
[78] Tsang A, Von Korff M, Lee S, Alonso J, Karam E, Angermeyer MC, Borges GL, Bromet EJ, Demytteneare K, de Girolamo G, de Graaf R, Gureje O, Lepine JP, Haro JM, Levinson D, Oakley Browne MA, Posada-Villa J, Seedat S, Watanabe M. Common chronic pain conditions in developed and developing countries: gender and age differences and comorbidity with depression-anxiety disorders. J Pain 2008;9(10):883-891.
[79] Tukiainen T, Villani AC, Yen A, Rivas MA, Marshall JL, Satija R, Aguirre M, Gauthier L, Fleharty M, Kirby A, Cummings BB, Castel SE, Karczewski KJ, Aguet F, Byrnes A, Consortium GT, Laboratory DA, Coordinating Center -Analysis Working G, Statistical Methods groups-Analysis Working G, Enhancing Gg, Fund NIHC, Nih/Nci, Nih/Nhgri, Nih/Nimh, Nih/Nida, Biospecimen Collection Source Site N, Biospecimen Collection Source Site R, Biospecimen Core Resource V, Brain Bank Repository-University of Miami Brain Endowment B, Leidos Biomedical-Project M, Study E, Genome Browser Data I, Visualization EBI, Genome Browser Data I, Visualization-Ucsc Genomics Institute UoCSC, Lappalainen T, Regev A, Ardlie KG, Hacohen N, MacArthur DG. Landscape of X chromosome inactivation across human tissues. Nature 2017;550(7675):244-248.
[80] Uchida H, Ma L, Ueda H. Epigenetic gene silencing underlies C-fiber dysfunctions in neuropathic pain. J Neurosci 2010;30(13):4806-4814.
[81] Uchida H, Matsushita Y, Ueda H. Epigenetic regulation of BDNF expression in the primary sensory neurons after peripheral nerve injury: implications in the development of neuropathic pain. Neuroscience 2013;240:147-154.

[82] Valtcheva MV, Copits BA, Davidson S, Sheahan TD, Pullen MY, McCall JG, Dikranian K, Gereau RWt. Surgical extraction of human dorsal root ganglia from organ donors and preparation of primary sensory neuron cultures. Nat Protoc 2016;11(10):1877-1888.
[83] Wei M, Li L, Zhang Y, Zhang ZJ, Liu HL, Bao HG. LncRNA X inactive specific transcript contributes to neuropathic pain development by sponging miR-154-5p via inducing toll-like receptor 5 in CCI rat models. J Cell Biochem 2019;120(2):1271-1281.
[84] Wen X, Luo Z, Zhao W, Calandrelli R, Nguyen TC, Wan X, Charles Richard JL, Zhong S. Single-cell multiplex chromatin and RNA interactions in ageing human brain. Nature 2024.
[85] Woodson CM, Kehn-Hall K. Examining the role of EGR1 during viral infections. Front Microbiol 2022;13:1020220.
[86] Xu Z, Lee MC, Sheehan K, Fujii K, Rabl K, Rader G, Varney S, Sharma M, Eilers H, Kober K, Miaskowski C, Levine JD, Schumacher MA. Chemotherapy for pain: reversing inflammatory and neuropathic pain with the anticancer agent mithramycin A. Pain 2024;165(1):54-74.
[87] Yan F, Powell DR, Curtis DJ, Wong NC. From reads to insight: a hitchhiker's guide to ATAC-seq data analysis. Genome Biol 2020;21(1):22.
[88] Yang L, Xu M, Bhuiyan SA, Li J, Zhao J, Cohrs RJ, Susterich JT, Signorelli S, Green U, Stone JR, Levy D, Lennerz JK, Renthal W. Human and mouse trigeminal ganglia cell atlas implicates multiple cell types in migraine. Neuron 2022;110(11):1806-1821 e1808.
[89] Yu S, Chen C, Pan Y, Kurz MC, Datner E, Hendry PL, Velilla MA, Lewandowski C, Pearson C, Domeier R, McLean SA, Linnstaedt SD. Genes known to escape X chromosome inactivation predict co-morbid chronic musculoskeletal pain and posttraumatic stress symptom development in women following trauma exposure. Am J Med Genet B Neuropsychiatr Genet 2019;180(6):415-427.
[90] Zaghlool A, Niazi A, Bjorklund AK, Westholm JO, Ameur A, Feuk L. Characterization of the nuclear and cytosolic transcriptomes in human brain tissue reveals new insights into the subcellular distribution of RNA transcripts. Sci Rep 2021;11(1):4076.
[91] Zhang H, Song L, Wang X, Cheng H, Wang C, Meyer CA, Liu T, Tang M, Aluru S, Yue F, Liu XS, Li H. Fast alignment and preprocessing of chromatin profiles with Chromap. Nat Commun 2021;12(1):6566.

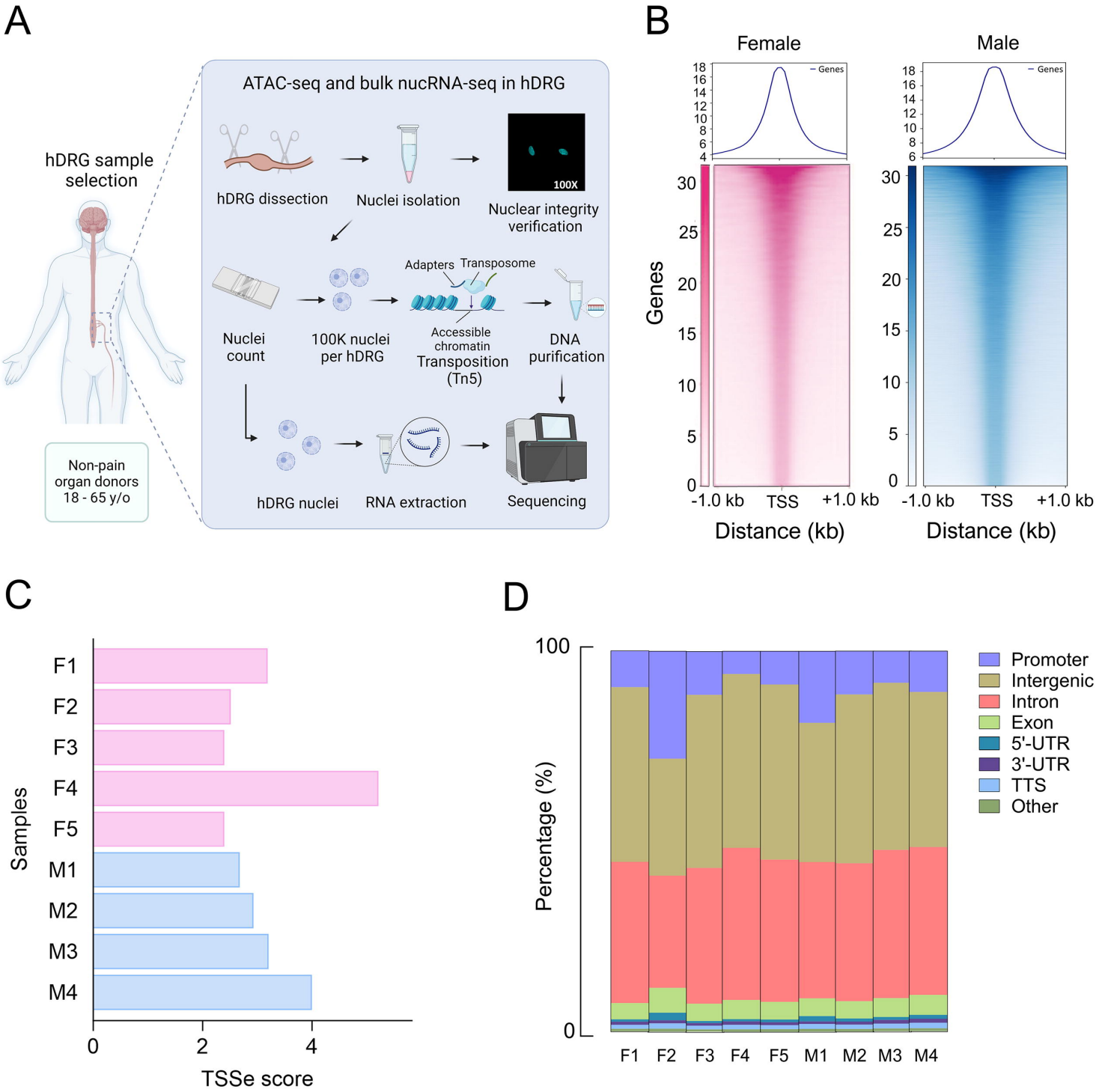
A
hDRG sample selection
Non-pain organ donors 18 - 65 y/o
ATAC-seq and bulk nucRNA-seq in hDRG
hDRG dissection
Nuclei isolation
100X
Nuclear integrity verification
Nuclei count
100K nuclei per hDRG
Adapters
Transposome
Accessible chromatin
Transposition (Tn5)
DNA purification
hDRG nuclei
RNA extraction
Sequencing
B
Female
Male
Genes
Genes
Genes
-1.0 kb
TSS
+1.0 kb
Distance (kb)
C
Samples
F1
F2
F3
F4
F5
M1
M2
M3
M4
TSSe score
D
Percentage (%)
Promoter
Intergenic
Intron
Exon
5'-UTR
3'-UTR
TTS
Other

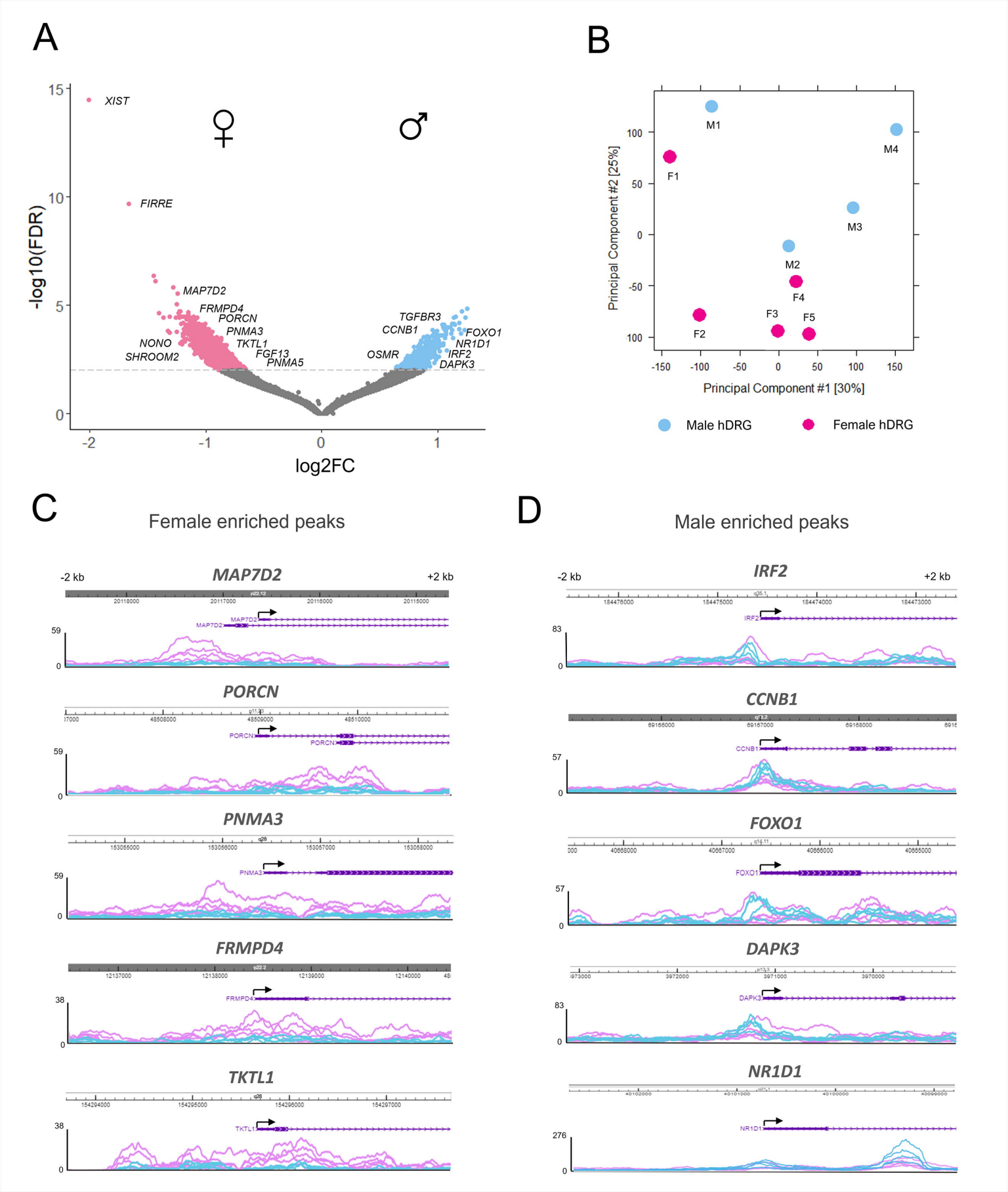
A
XIST
FIRRE
MAP7D2
FRMPD4
PORCN
PNMA3
TKTL1
FGF13
PNMA5
NONO
SHROOM2
TGFBR3
CCNB1
FOXO1
NR1D1
IRF2
DAPK3
OSMR
-log10(FDR)
log2FC
B
M1
M2
M3
M4
F1
F2
F3
F4
F5
Principal Component #2 [25%]
Principal Component #1 [30%]
Male hDRG
Female hDRG
C
Female enriched peaks
-2 kb
+2 kb
MAP7D2
PORCN
PNMA3
FRMPD4
TKTL1
D
Male enriched peaks
IRF2
CCNB1
FOXO1
DAPK3
NR1D1

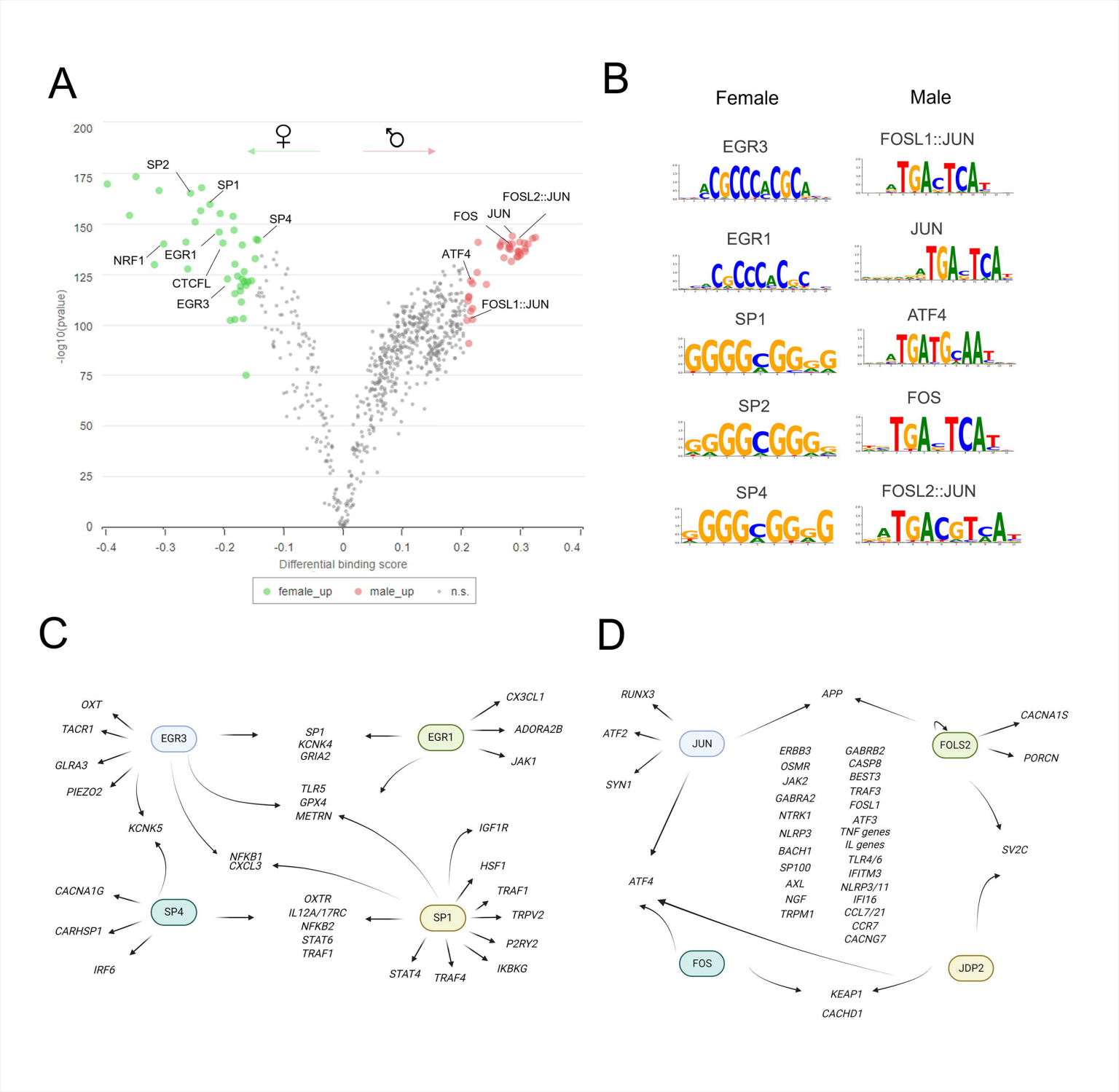
A
♀
♂
SP2
SP1
SP4
NRF1
EGR1
CTCFL
EGR3
FOS
JUN
FOSL2::JUN
ATF4
FOSL1::JUN
-log10(pvalue)
Differential binding score
female_up
male_up
n.s.
B
Female
Male
EGR3
FOSL1::JUN
EGR1
JUN
SP1
ATF4
SP2
FOS
SP4
FOSL2::JUN
C
OXT
TACR1
GLRA3
PIEZO2
EGR3
KCNK5
SP1
KCNK4
GRIA2
EGR1
CX3CL1
ADORA2B
JAK1
TLR5
GPX4
METRN
NFKB1
CXCL3
IGF1R
HSF1
TRAF1
TRPV2
P2RY2
IKBKG
TRAF4
STAT4
CACNA1G
CARHSP1
IRF6
SP4
OXTR
IL12A/17RC
NFKB2
STAT6
TRAF1
SP1
D
RUNX3
ATF2
SYN1
JUN
APP
ERBB3
OSMR
JAK2
GABRA2
NTRK1
NLRP3
BACH1
SP100
AXL
NGF
TRPM1
GABRB2
CASP8
BEST3
TRAF3
FOSL1
ATF3
TNF genes
IL genes
TLR4/6
IFITM3
NLRP3/11
IFI16
CCL7/21
CCR7
CACNG7
FOLS2
CACNA1S
PORCN
SV2C
ATF4
FOS
KEAP1
CACHD1
JDP2

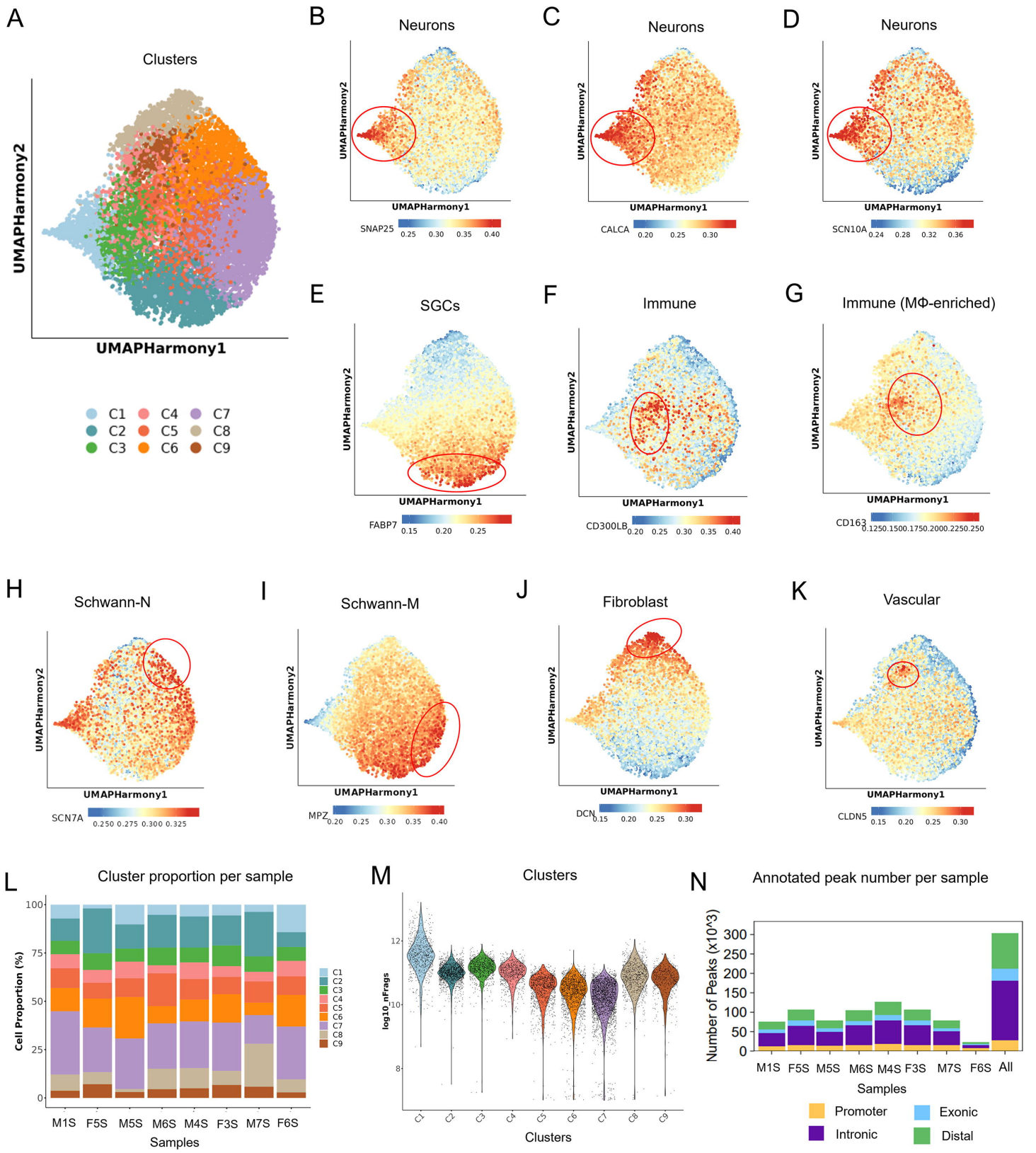
A
Clusters
UMAPHarmony2
UMAPHarmony1
C1 C4 C7
C2 C5 C8
C3 C6 C9
B
Neurons
SNAP25
0.25 0.30 0.35 0.40
C
Neurons
CALCA
0.20 0.25 0.30
D
Neurons
SCN10A
0.24 0.28 0.32 0.36
E
SGCs
FABP7
0.15 0.20 0.25
F
Immune
CD300LB
0.20 0.25 0.30 0.35 0.40
G
Immune (MΦ-enriched)
CD163
0.1250.1500.1750.2000.2250.250
H
Schwann-N
SCN7A
0.250 0.275 0.300 0.325
I
Schwann-M
MPZ
0.20 0.25 0.30 0.35 0.40
J
Fibroblast
DCN
0.15 0.20 0.25 0.30
K
Vascular
CLDN5
0.15 0.20 0.25 0.30
L
Cluster proportion per sample
Cell Proportion (%)
0 25 50 75 100
M1S F5S M5S M6S M4S F3S M7S F6S
Samples
C1 C2 C3 C4 C5 C6 C7 C8 C9
M
Clusters
log10_nFrags
8 10 12
C1 C2 C3 C4 C5 C6 C7 C8 C9
Clusters
N
Annotated peak number per sample
Number of Peaks (x10^3)
0 50 100 150 200 250 300
M1S F5S M5S M6S M4S F3S M7S F6S All
Samples
Promoter
Exonic
Intronic
Distal

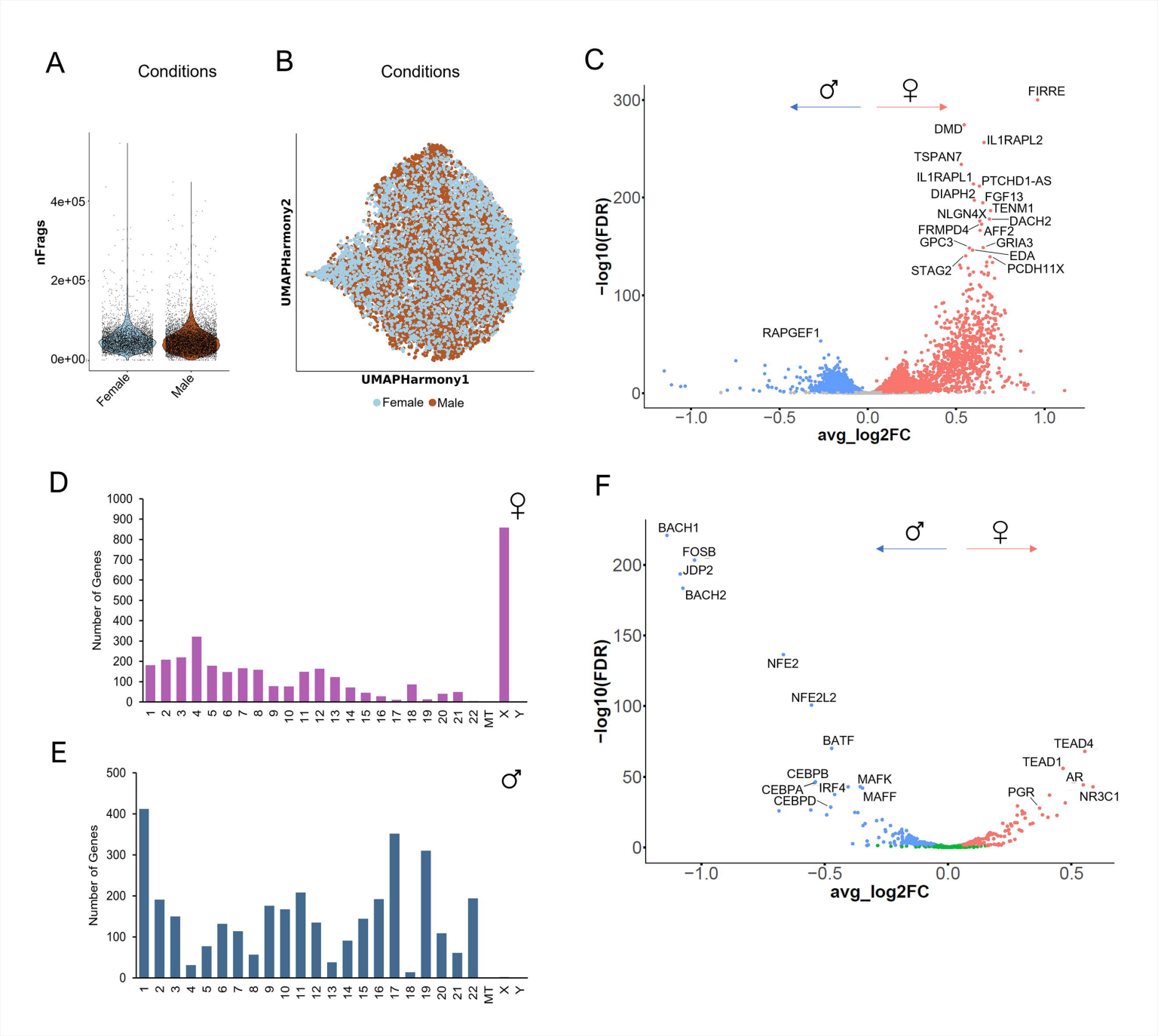
A
Conditions
nFrags
4e+05
2e+05
0e+00
Female
Male
B
Conditions
UMAPHarmony2
UMAPHarmony1
Female
Male
C
♂
♀
FIRRE
DMD
IL1RAPL2
TSPAN7
IL1RAPL1
PTCHD1-AS
DIAPH2
FGF13
TENM1
NLGN4X
DACH2
FRMPD4
AFF2
GPC3
GRIA3
EDA
STAG2
PCDH11X
RAPGEF1
−log10(FDR)
avg_log2FC
D
Number of Genes
♀
E
Number of Genes
♂
F
BACH1
FOSB
JDP2
BACH2
NFE2
NFE2L2
BATF
TEAD4
TEAD1
AR
NR3C1
PGR
CEBPB
CEBPA
IRF4
CEBPD
MAFK
MAFF
−log10(FDR)
avg_log2FC

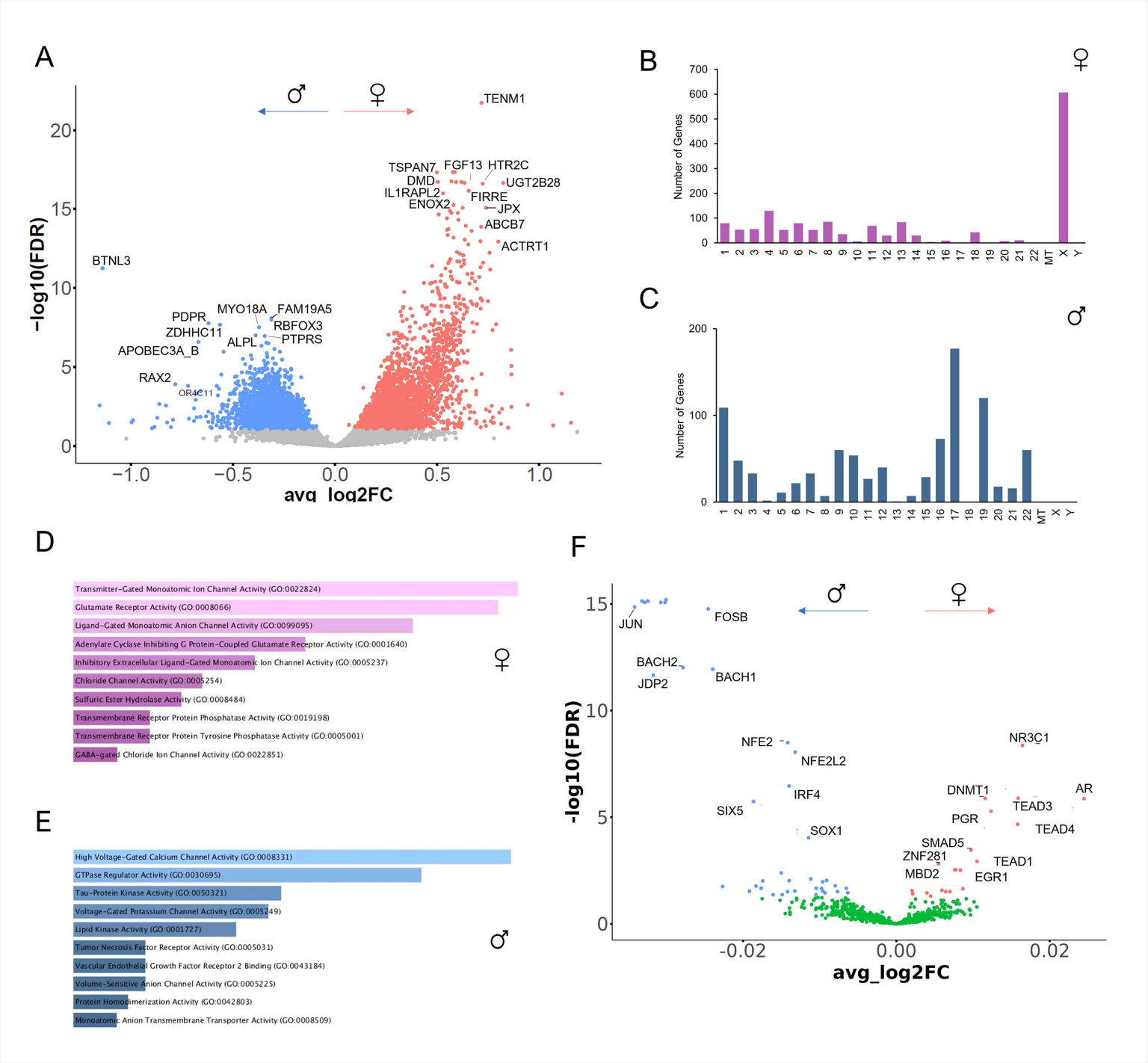
A
♂
♀
TENM1
TSPAN7
FGF13
HTR2C
DMD
UGT2B28
IL1RAPL2
FIRRE
ENOX2
JPX
ABCB7
ACTRT1
BTNL3
PDPR
MYO18A
FAM19A5
RBFOX3
ZDHHC11
ALPL
PTPRS
APOBEC3A_B
RAX2
OR4C11
-log10(FDR)
avg_log2FC
B
♀
Number of Genes
C
♂
Number of Genes
D
Transmitter-Gated Monoatomic Ion Channel Activity (GO:0022824)
Glutamate Receptor Activity (GO:0008066)
Ligand-Gated Monoatomic Anion Channel Activity (GO:0099095)
Adenylate Cyclase Inhibiting G Protein-Coupled Glutamate Receptor Activity (GO:0001640)
Inhibitory Extracellular Ligand-Gated Monoatomic Ion Channel Activity (GO:0005237)
Chloride Channel Activity (GO:0005254)
Sulfuric Ester Hydrolase Activity (GO:0008484)
Transmembrane Receptor Protein Phosphatase Activity (GO:0019198)
Transmembrane Receptor Protein Tyrosine Phosphatase Activity (GO:0005001)
GABA-gated Chloride Ion Channel Activity (GO:0022851)
♀
E
High Voltage-Gated Calcium Channel Activity (GO:0008331)
GTPase Regulator Activity (GO:0030695)
Tau-Protein Kinase Activity (GO:0050321)
Voltage-Gated Potassium Channel Activity (GO:0005249)
Lipid Kinase Activity (GO:0001727)
Tumor Necrosis Factor Receptor Activity (GO:0005031)
Vascular Endothelial Growth Factor Receptor 2 Binding (GO:0043184)
Volume-Sensitive Anion Channel Activity (GO:0005225)
Protein Homodimerization Activity (GO:0042803)
Monoatomic Anion Transmembrane Transporter Activity (GO:0008509)
♂
F
♂
♀
JUN
FOSB
BACH2
JDP2
BACH1
NFE2
NFE2L2
NR3C1
IRF4
DNMT1
AR
SIX5
TEAD3
PGR
SOX1
TEAD4
SMAD5
ZNF281
TEAD1
MBD2
EGR1
-log10(FDR)
avg_log2FC

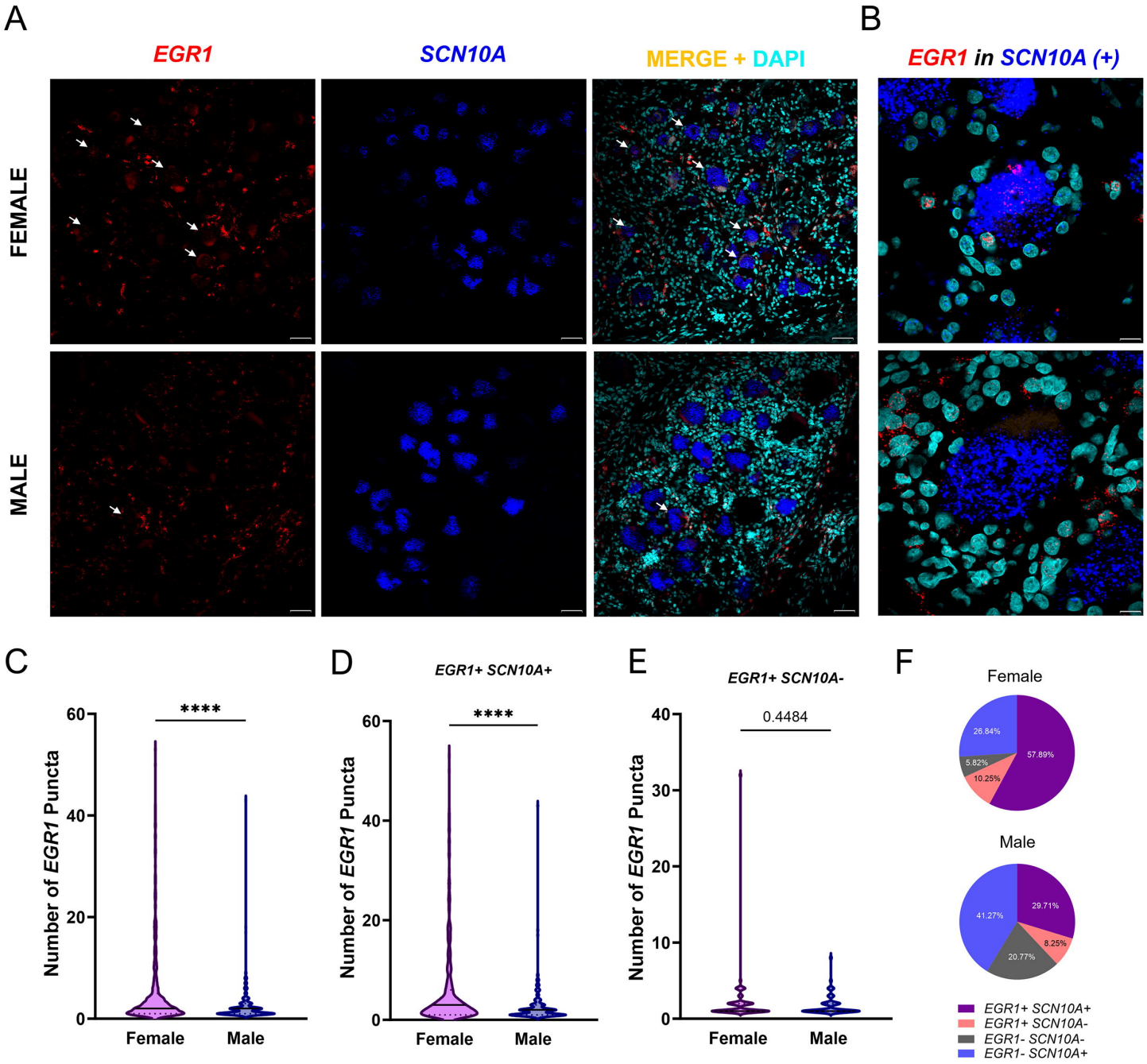
A
EGR1
SCN10A
MERGE + DAPI
B
EGR1 in SCN10A (+)
FEMALE
MALE
C
Number of EGR1 Puncta
****
Female
Male
D
EGR1+ SCN10A+
****
E
EGR1+ SCN10A-
0.4484
F
Female
26.84%
57.89%
5.82%
10.25%
Male
29.71%
41.27%
8.25%
20.77%
EGR1+ SCN10A+
EGR1+ SCN10A-
EGR1- SCN10A-
EGR1- SCN10A+

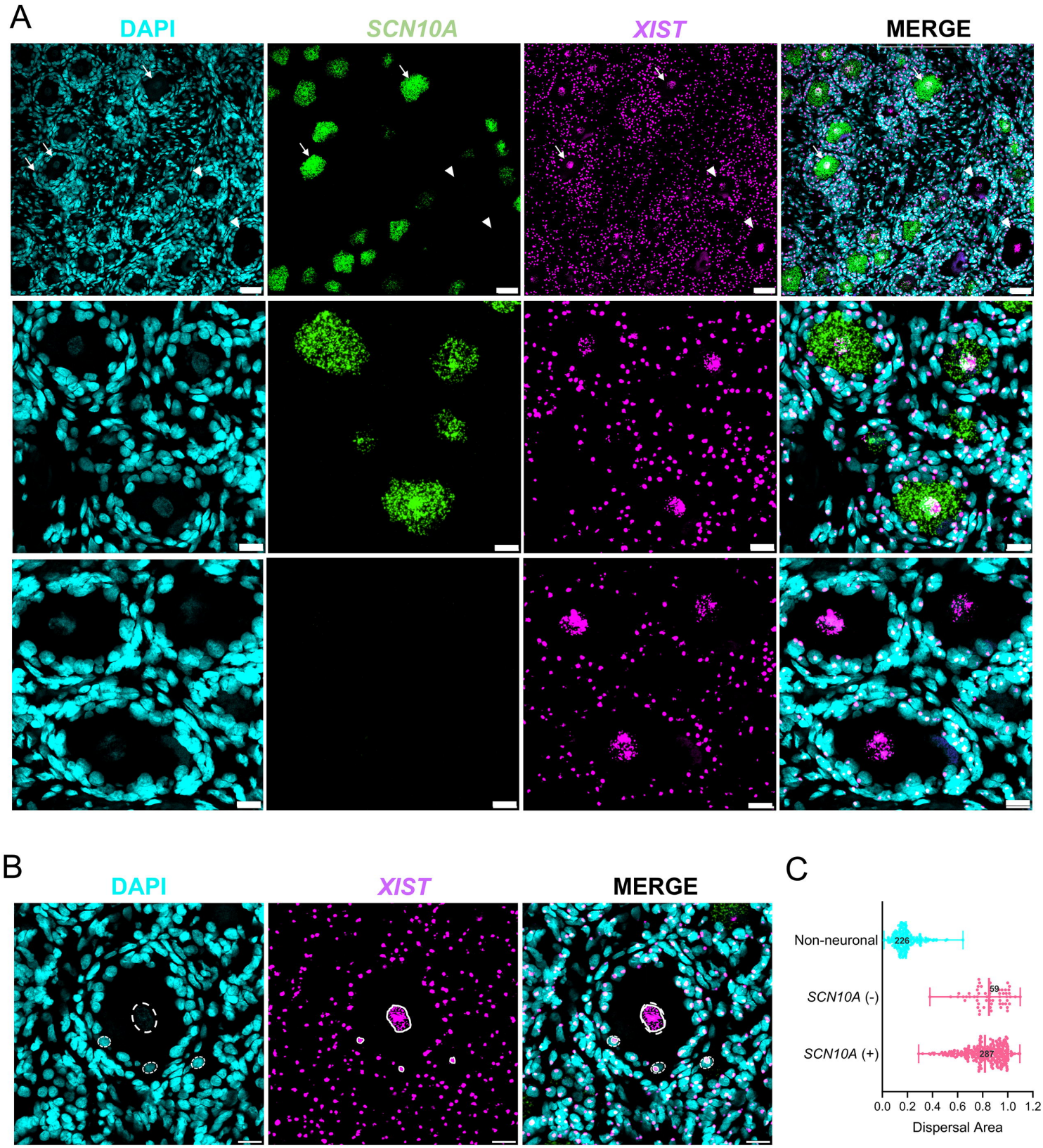
A
DAPI
SCN10A
XIST
MERGE
B
DAPI
XIST
MERGE
C
Non-neuronal
SCN10A (-)
SCN10A (+)
226
59
287
0.0
0.2
0.4
0.6
0.8
1.0
1.2
Dispersal Area